DIPLOMA THESIS

Implications of AGE cross-linking on the viscoelastic behavior in individual collagen Fibrils

carried out for the purpose of obtaining the degree of Master of Science, submitted at TU Wien, Faculty of Mechanical and Industrial Engineering by

Walaa Taha, BSc

09927199

Under the supervision of

Univ. Prof. Dipl. -Ing. Dr. sc. nat. Philipp Thurner

Dipl. -Ing. Manuel Rufin

Institute of Lightweight Design and Structural Biomechanics

Vienna, October 2022

Affidavit

I declare in lieu of oath, that I wrote this thesis and performed the associated research myself, using only literature cited in this volume. If text passages from sources are used literally, they are marked as such.

I confirm that this work is original and has not been submitted elsewhere for any examination, nor is it currently under consideration for a thesis elsewhere.
I acknowledge that the submitted work will be checked electronically-technically using suitable and state-of-the-art means (plagiarism detection software). On the one hand, this ensures that the submitted work was prepared according to the high-quality standards within the applicable rules to ensure good scientific practice "Code of Conduct" at the TU Wien. On the other hand, a comparison with other student theses avoids violations of my personal copyright.

———————————————   ———————————————

City and Date   *Signature*

Acknowledgement

First of all, I would like to give special thanks to my family for their support and constant encouragement to me to continue my studies. I would like to acknowledge and give my warmest thanks to Prof. Philipp Thurner, who gave me the chance to do my master's work in his institute with a wonderful team. A especial thank to my thesis advisor Dipl.-Ing. Manuel Rufin for his guidance, assistance, and constant support throughout the entire research work. I would also like to thank Dipl.-Ing. Mathis Nalbach and Dipl.-Ing. Magdalena Fuchs for their great assistance.

Appreciation is also extended to the members of the Institute of Lightweight Design and Structural Biomechanics and to my colleague Dipl.-Ing. Mercedes Spannagel.

Abstract

Collagenous tissues are essential and have great importance to the biomechanical integrity of the body. Collagen type I, among other collagen types of the collagen super family, is the major protein found in vertebrates and in higher invertebrates. Most of collagen-rich tissues exhibit a hierarchical structure with different mechanical behavior at each individual level. At the nano level, collagen fibrils are the functional and basic building blocks in these tissues. Collagen cross-linking affects the mechanical properties of the fibrils. Advanced Glycation End products (AGEs) are products resulting from non-enzymatic cross-linking, a process known as glycation and leads to stiffening of the fibrils, which may cause whole tissue deterioration.

In this thesis a study is performed on collagen fibrils extracted from a wild type (WT) mouse tail tendon to examine the effect of glycation on their viscoelastic behavior. Two types of mechanical measurements were accomplished: Atomic Force Microscopy (AFM) dynamic nanoindentation and dynamic tensile tests using a novel instrument with quick sample loading and unloading. Both measurements were executed on the same fibrils from the same tendon fascicle, in phosphate buffered saline (PBS) to simulate the physiological environment. A test group was prepared by glycating collagen fibrils with Methylglyoxal (MGO) to mimic the physiological effects of the AGEs in aging and pathology. Another group was prepared from the same tendon fascicle as a control group to reduce any systematic errors or any differences that are not related to glycation. AFM dynamic nanoindentation measurements in PBS were performed on both groups (N= 10 in each group) before and after incubation. Afterwards dynamic tensile tests were conducted on both groups also in PBS to investigate the viscoelastic behavior of both groups in their normal loading direction (the long axis).

Through the combination of the two methods, different parameters such as loss and storage modulus, loss tangent, dynamic modulus and ultimate strength could be measured and investigated to assess the effect of AGEs on nanomechanics at the collagen fibril-level.

Comparing both methods, the AFM dynamic nanoindentation is a powerful method, in which different experiments can be conducted using different protocols (e.g., stress relaxation

experiments, creep experiments, etc.) with a large range of forces and frequencies. The measurements on the fibrils are reproducible and can be conducted several times with different configurations on the very same spot on the fibril. Despite these benefits one of the shortcomings of this method is the low acquisition speed resulting in long measurement times that can last for hours. Also, an important range of frequencies less than 0.5 Hz, which simulates quasi-static tests and reveals more the viscous behavior of the sample is hard to be investigated using the AFM nanoindentation as the measurements at this range are very noisy.

On the other hand, the dynamic tensile testing measurement using NanoTens device is easy to conduct with fast sample loading and unloading. It can be performed in a very short time (5 minutes per fibril) compared to AFM. The measurements are also reproducible unless the fibril ruptures, which needs some expertise to be avoided. The shortcoming of this method is the extra sample preparation, which must be conducted with certain conditions to make the loading of the fibril on the microgripper easy and possible. While the lower frequencies (< 0.5 Hz) are more feasible than with AFM, higher frequencies (> 2 Hz) cannot be examined using this method.

The results of the analyzed data of both experiments correlated but could not give clear evidence on the influences of glycation on the viscoelastic behavior at the nanoscale of collagen fibrils. Although the glycated fibrils seemed to be less viscous than the control group and the ultimate strength of the glycated fibrils showed higher values at lower strain compared to the untreated ones, this may not be directly related to glycation.

Table of Contents

1   Introduction

The mechanical properties and function of the human skeletal system depend on the collagen fibrils, which are the functional and basic building block in collagens tissues. They support mechanical strength giving and maintaining form, while also providing flexibility to different organs of the body. Various structural characteristics of collagen-based tissues give them mechanical properties relevant to their widely different functions. Several factors play a role in determining the mechanical strength of the tissue. On one side is the content of collagen, where on the other side the orientation of the fibrils, which varies markedly between tissues. For example, in skin, collagen fibrils are differently oriented compared to fibrils in tendons, which permits large extension of the tissue until the fibrils themselves are loaded. While in tendons they are aligned in parallel and hence loaded immediately, allowing maximum transfer of the energy produced by muscle contraction to the skeletal system. [1]

The deleterious changes in collagen due to aging and diabetes mellitus, which manifest in different collagenous tissues are a result of the intermolecular cross-linking of collagen and generation of adducts, known as glycation, within the tissues. Stiffening and dysfunction of the joints, the vascular system, the renal and retinal capillaries, tendons, and bones follow similar patterns. The process is accelerated in diabetic patients due to hyperglycemia and is considered the main cause of the premature morbidity and mortality.[2] Stiffening of these tissues leads to an increased rate of injury and degeneration. In musculoskeletal tissues for example, 75% of people over the age of 65 will suffer an injury due to tissue degeneration. While many mechanisms contribute to this link between age and degeneration, progressive accumulation of AGEs is one of the most prominent mechanisms believed to be responsible. Due to the high content of collagen in connective tissues, age-related changes in collagen-mechanics, that may lead to increased risk of injury and degeneration have been linked to the presence of AGEs.[3]

A heterogeneous group of compounds that include more than 20 different products, called advanced glycation end products (AGEs), is a result of the classical Maillared reaction discovered at the beginning of 20th century. It is a complex series of sequential reactions

between glucose and long-lived proteins like collagen. The accumulation of AGEs and their functionally compromised adducts are linked to the changes seen during aging and for the development of many age-related diseases, such as diabetes, atherosclerosis, as well as oxidative stress and inflammation associated with neurodegenerative diseases of aging. Chronic hyperglycemia results in several metabolic and biochemical disturbances including increase of a series of highly reactive α-dicarbonyl compounds like Methylglyoxal (MGO), which is 2 to 3 orders of magnitude more reactive than glucose. Other crucial AGEs compounds are glucosepane and Nε-carboxymethyl-lysine (CML). AGEs formation leads to irreversible changes to the biological tissues as they alter their structural and functional integrity.[3]

The functional consequences of AGEs in connective tissues and their role in the onset and progression of connective tissue diseases are complex and still an open question. These consequences can be divided into two functional classes, biological and mechanical. Biologically, formation of AGEs leads to dramatic modification of the interactions between collagen and other molecules like proteoglycans, enzymes, and cell integrins. Collagen surface is modified by AGEs and cell-matrix interactions are affected leading to wound heal inhibition and inflammation. Biomechanically, the non-enzymatic intermolecular cross links modify the physical properties of collagen, leading to higher: stiffness, failure loads, and denaturation temperatures. On the level of the whole tissue, an increase in tissue fragility is observed.[4]

1.1 Aim of thesis

The objective of this thesis is to further study the effects of glycation on collagen fibrils. As a complementary study to a previous work done on collagen fibrils extracted from a WT mouse tail tendon, which investigated the effects of glycation on surface charge as well as indentation stiffness. This study aims to have a better understanding of the implications of glycation on the viscoelastic behavior in individual collagen fibrils, which has not yet been examined. Methylglyoxal (MGO), a high reactive α-dicarbonyl late by product of the Maillard reaction is used for in vitro glycation of individual collagen fibrils from WT mouse tail tendon.

Two different methods were used in this thesis on the same collagen fibrils of both a control and an MGO cross-linked group, to explore for the first time the implication of glycation on the viscoelastic behavior of the fibrils.

Despite the wide use of AFM for mechanical characterization of biological tissues, most of the earlier studies performed on the nanoscale, measured solely the apparent elastic modulus of the samples, disregarding viscoelastic behavior.[5] AFM was used in the current work as it is a versatile device capable of applying and measuring nano- and pico- Newton forces on soft, biological materials in their native state. Dynamic nanoindentation analysis provides a more robust way of investigating the viscoelastic nature of the fibrils.

Additionally, dynamic tensile tests were performed on the same fibrils in their loading direction (long axis), using a novel instrument with quick sample loading, and unloading.

1.2   Structure of thesis

Chapter 2 gives a general introduction about collagen-rich tissues, collagen fibrils and the role of collagen cross-linking. The mechanical aspects of biological tissues are then briefly discussed at the end this chapter focusing on connective tissues and their viscoelasticity. In chapter 3 an overview of the atomic force microscopy AFM is presented, including the working principle of the measurement method used in this study. Chapter 4 explains the study design of this thesis, starting with sample preparation, AFM dynamic nanoindentation method and ending with the dynamic tensile testing. The results and the analysis of both experiments are presented in chapter 5, followed by chapter 6 with a brief discussion and interpretation. A conclusion of this thesis as well as future suggestions are given in chapter 7.
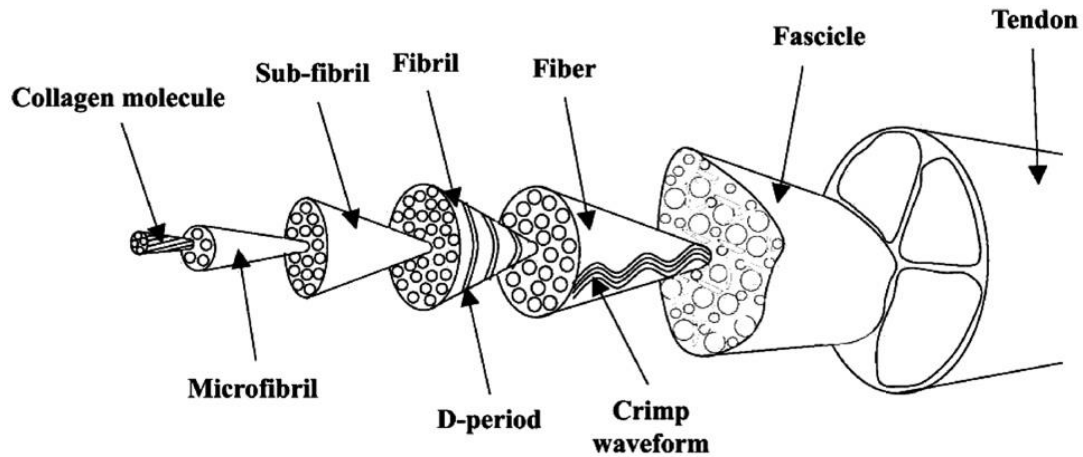
2 Collagen

2.1 Collagen-rich tissues

Among different proteins in mammals, collagen type I is the major constituent and the most abundant protein found in various tissues such as tendons, ligaments, bone, skin, and dentin. It plays an essential role in arteries, the cornea and in most of the extracellular matrix in general.[6] Collagen type I belongs to a super-family containing 28 different types of collagen that have been discovered to date in vertebrates and higher invertebrates. The combination of collagen type I with other collagenous and non-collagenous molecules such as proteoglycans leads to the formation of a variety of tissue scaffolds giving them their load-bearing mechanical properties.[7] Collagen type I provides mechanical stability, strength and toughness to the different collagenous tissues for their distinct mechanical requirements and the different functions they must fulfill. Tendons and ligaments for example are needed to transfer forces from muscles to the bones and to store elastic energy for high-performance locomotion, while skin and artery walls need to be flexible and resistant to pressure. This requires that collagen combines with other molecules in various different arrangements. In order to function properly, even muscles need a scaffold rich of collagen wherein muscle cells can be embedded.[6]

Collagen-rich tissues are essential and have great significance to the biomechanical integrity of the body. A hierarchical structure can be observed in most of these tissues with differences in the mechanical properties in the discrete levels.[8]

Tendons for example, exhibit a particular and well-organized hierarchical structure as seen in Figure 1. Starting from the macro-scale represented in a whole tendon , which is further subdivided into large fascicles with diameters of 80-320 µm, down to collagen fibers with 1-10 µm diameter, to collagen fibrils with diameters of 50-500 nm, reaching the basic collagen monomers with 1.6 nm diameter and 300 nm length.[9, 10]

Figure 1: Tendon's hierarchical structure, showing the individual levels from the whole tendon to collagen molecule.[11]

The differences in the mechanical properties between the individual levels originate in the force transfer between the subunits from the lower hierarchical levels to the higher ones. In order to reveal how this force is transferred it is important to understand the mechanical behavior of each separate level.[8] Among the different levels Collagen fibrils are of great interest to study as they form the basic building block in the different collagen-based tissues.

2.1.1 Collagen molecules and fibrils

The collagen molecule, also called tropocollagen is a 300 nm long triple helix with a diameter of 1.6 nm as illustrated in Figure 2a. It has a spatial arrangement of three polypeptide chains, wound around each other in a helical structure as in Figure 2b and is stabilized by hydrogen bonding. Each polypeptide chain is a repeating amino acid pattern of $(Gly\text{-}X\text{-}Y)_n$, where Gly is glycine and X and Y are other amino acids like proline, hydroxyproline, alanine or glutamic acid. [12] The ends of the tropocollagen are made by telopeptides, which are a non-helical N- and C- terminals.[13]
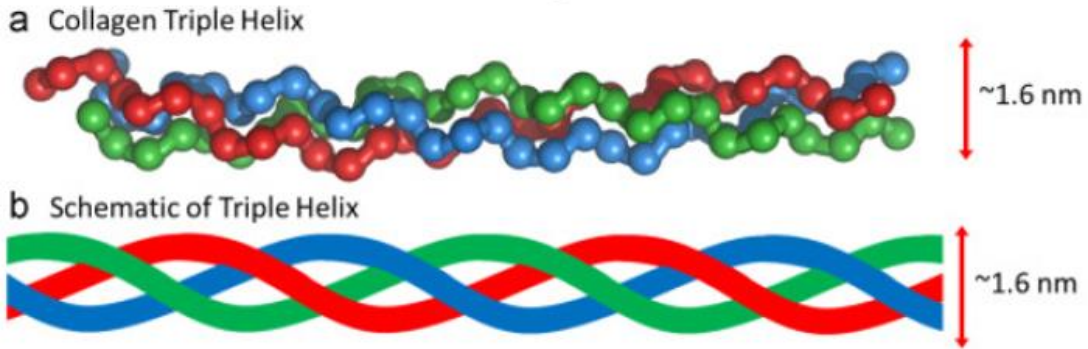
Figure 2: a schematic of tropocollagen showing the spatial arrangement of the three polypeptide chains **[14]**

These triple helices (tropocollagen) assemble into collagen fibrils in an arrangement such that for example the N-termini of two laterally adjacent triple helices are separated by 67 nm as seen in Figure 3. This staggered arrangement leads to the formation of alternating regions of low and high protein density (gaps and overlaps) along the fibril axis. [7] This repeating banding pattern is called D-banding and characterizes the collagen fibrils. [6] It appears as an alternating dark and light regions in transmission electron microscopy (TEM), while in atomic force microscopy (AFM) it can be seen as peaks and valleys along the fibril with minimum to maximum difference between 1-~6 nm, depending on the hydration state as shown in Figure 4.[7]
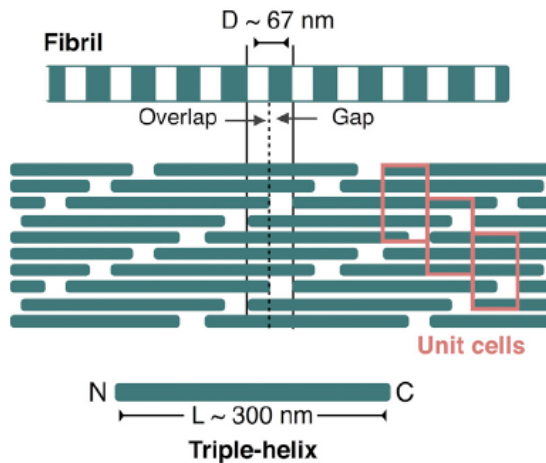
Figure 3: Structural hierarchy of type I collagen fibril, showing the gap and overlap regions. [7]

Collagen fibrils are the functional and basic building blocks within any collagenous connective tissue, they provide tensile strength and elasticity to these tissues.[4] Due to the structure and shape of collagen molecules, fibrils have a single preferred loading direction, which is along their longitudinal axis.[15] They have thicknesses ranging from 50 nm to a few hundred nanometers with lengths up to millimeters. The inter-molecular bonds like Van der Waals, hydrogen bonds, intra and inter-molecular cross-links as well as hydration strongly affect the structure and mechanical behavior of the collagen fibrils. [12, 15] Although many studies and experiments were performed for decades at the higher hierarchical levels e.g. the macro-scale, direct measurements on the lower levels such as the level of individual collagen fibrils have only recently become possible with the advent of nanotechnology, especially atomic force microscopy (AFM) and the development of dedicated measurement protocols and devices.[10]
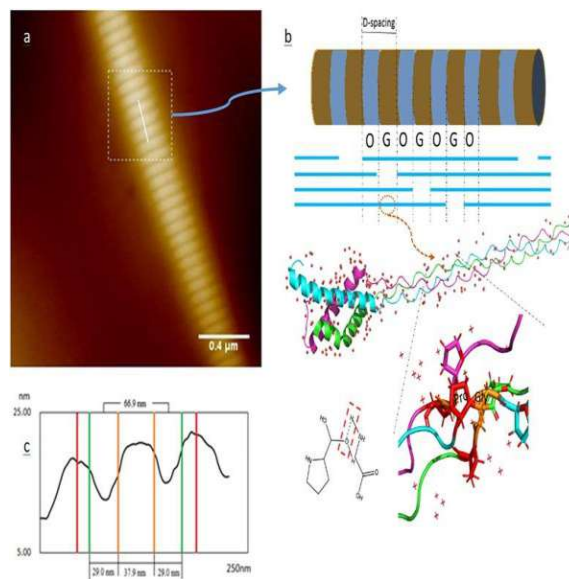
Figure 4: an image of a collagen fibril from a bovine tendon using atomic force microscopy [16]

2.1.2 Collagen cross-linking

Mechanical properties of collagen-rich tissues are highly dependent on the intermolecular cross-links between collagen molecules, they preserve the mechanical integrity and structural stability of these tissues. Although cross-linking development depends on the tissue and on the type of loading the tissue goes through, certain types of collagen cross-links are essential to proper function, while others can cause tissue deterioration. Hence, cross-linking involves

two different mechanisms of cross-link formation, the enzymatic cross-link and the nonenzymatic cross-link. [15, 17]

Enzymatic intermolecular cross-linking

This type of crosslinking represents an important step in development and repair of collagen connective tissues. It is essential to proper function of the tissue as it promotes strength, stiffness and the resistance of the tissue to failure.[4] It is a precisely controlled enzymatic process driven by a family of enzymes like lysyl oxidase and lysyl hydroxylase. Both enzymes act on lysine or hydroxylysine in the telopeptide part of the collagen molecule and regulates the robust formation of stable inter molecular collagen cross-links during fibril development and maturation. One of the characteristics of type I collagen is excessive post-translational modification. While lysine residues can be converted to the respective aldehyde by lysyl oxidase, hydroxylation is the key to cross-linking of collagen, which is catalyzed by lysyl hydroxylase (LH) [4, 15, 17, 18]

Non enzymatic cross-linking

Although enzymatic cross-linking reaches plateaus at maturation, a further rise of connective tissue stiffness has been recognized in elders and patients suffering from diabetes. This increase in tissue stiffening is associated with progressive collagen non-enzymatic cross-linking.[4] A process referred to as glycation, following maturation of the tissue involves a reaction with glucose and subsequent oxidation products, which leads to dysfunction of the collagenous tissues in old age. This can be explained as a result to reduced side-by-side sliding of collagen molecules in favor to lateral molecular interconnectivity by AGEs. The process is accelerated in diabetes due to higher amounts of glucose being present in tissues.[17, 19]

This reaction begins with the formation of a reversible Schiff-base between a carbohydrate, normally glucose, and a protein amino group like a lysine sidechain. Over a period of months to years a complex series of reactions result in metabolic by-products of glycolysis such as methyl glyoxal (MGO) (the cross-linking agent used in the current work), which can interact with the extracellular proteins and form advanced glycation end- products (AGEs) as shown

in Figure 5. Glucosepane is one of the most abundant AGEs found in collagen tissues, while MODIC and MOLD, which are an MGO-derived cross-links, are also found in collagen tissues but with less concentrations than glucosepane.[4, 12]
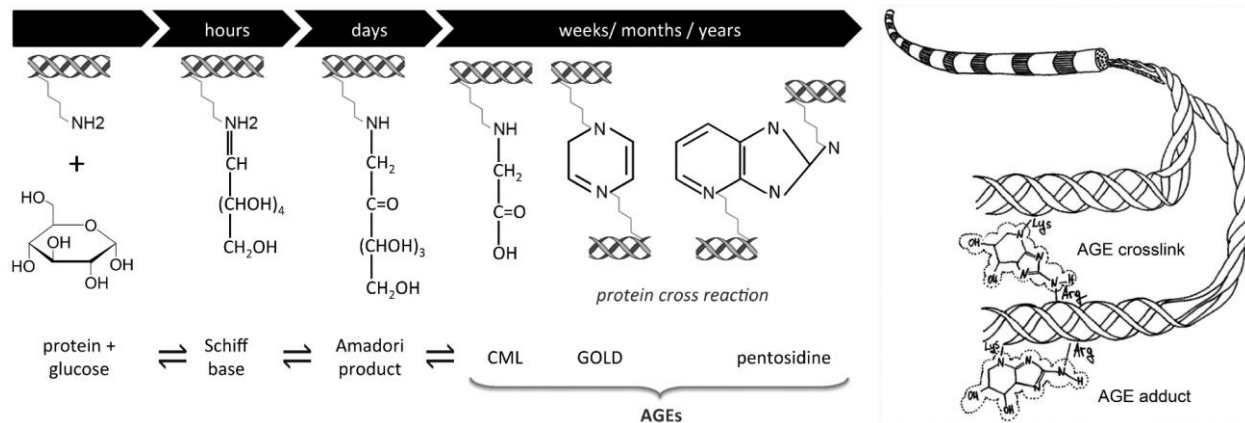
Figure 5: the sequence of chemical reactions and the formation the AGEs end products of glycation [4]

AGEs play an important role in tissue deterioration, they affect collagenous tissues mechanically and biologically regarding cell interaction. Mechanically, at the tissue level, the viscoelastic properties are highly affected and deviate from the less non-enzymatically cross-linked tissues. A significant increase in stiffness, toughness, ultimate strength and in the mechanical fragility has been observed in tendons through several studies.[4, 12] At the nano-level, collagen fibrils showed a significant increase in the stiffness due to glycation in a previous study. The results of this previous study are shown in Figure 6.[12]
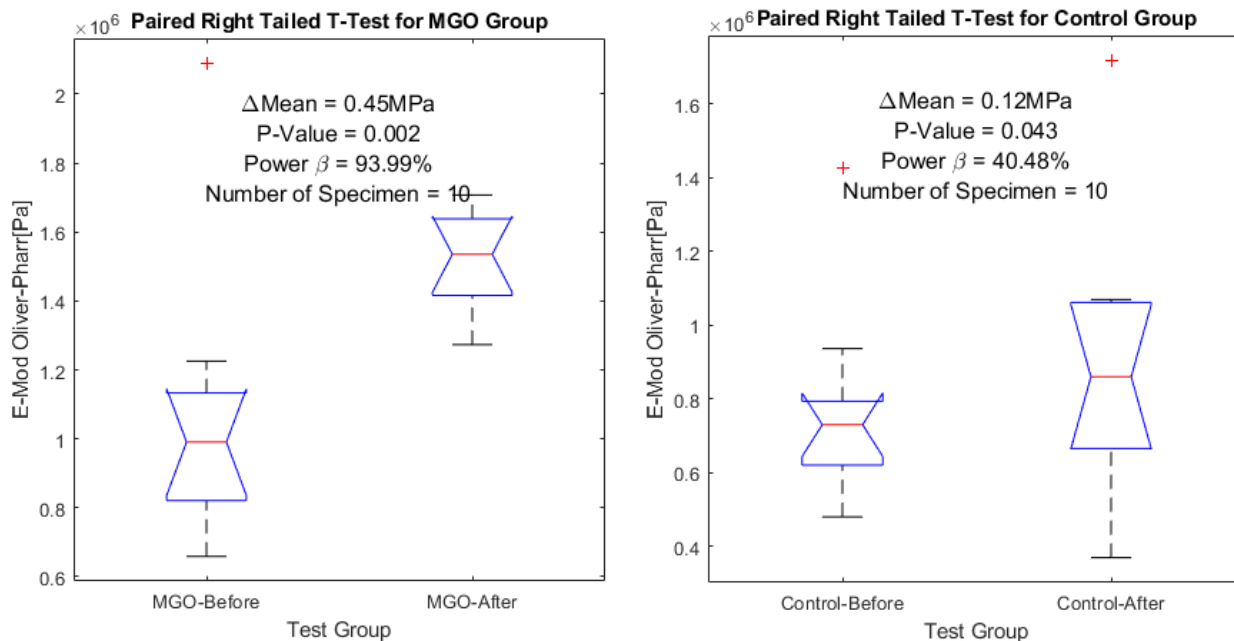
Figure 6:   Boxplots show the change in the indentation modulus after glycation process [12]

Biologically, glycation not only affects the protein-protein but, importantly, also protein (collagen)-cell interactions. AGEs modify the collagen surface and affect the cell-matrix interaction leading to an inhibition of wound repair and exacerbated inflammation. Integrins are a major link between cells and the ECM (extra cellular matrix), by sensing their microenvironment and signaling outside-in. Through integrins cells can apply forces to the ECM and vice versa. In case of glycation the polar properties of tropocollagen molecules are changed, which may affect the non-covalent binding to cells through the transmembrane integrin receptors leading to reduction in cell adhesion, migration and collagen turnover.[12, 20]

2.2   Mechanical characteristics of collagen-rich tissues

As mentioned before, collagen molecules exist in every connective tissue, but most of these tissues have different compositions. Previous studies based on tensile testing showed that the variation in the composition results in different mechanical behavior. When for example, comparing bones (contain minerals) and tendons, where both are composed mainly of collagen type I, huge differences in the mechanical behavior can be observed on the macro scale level. Although both tissues have the same parallel orientation of fibrils that leads to

transverse isotropic behavior, both materials have different mechanical response to loading. This can be explained due to the presence of minerals in bone while elastin is present in tendons. [15] Figure 7 shows the significant difference in the elastic modulus between bones and tendons. While bones have an elastic modulus of about 20 GPa, tendons have an elastic modulus one order of magnitude lower, with values of about 1 GPa.
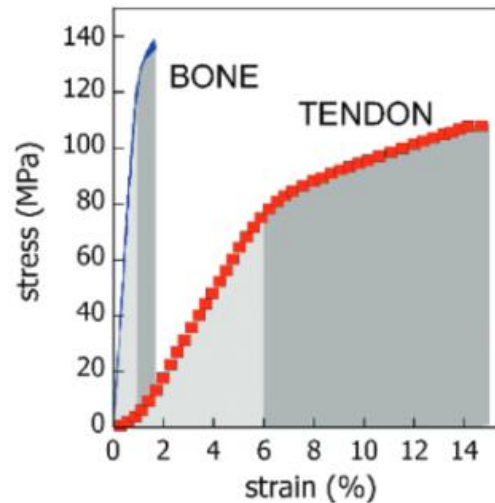

Figure 7:   stress-strain curves of both bone and tendon showing the significant difference in mechanical behavior [21]

Despite the differences in the mechanical behavior in collagenous tissues, they still have many properties in common. They can be considered viscoelastic materials when bones and dentin are excluded because of their mineralization. [12]

Regarding the lower hierarchical levels, a proposed mechanism to describe their behavior is that it depends on initial straightening of kinks in tropocollagen molecules at small strains, in what is called the toe region showed in Figure 8 (green arrows). This is followed by the axial stretching and molecular uncoiling, where the molecular sliding between molecules is dominant and presented by the linear region. This behavior is affected due to glycation as can be seen in Figure 8, as the glycated fibril shows to have increased mechanical parameters (failure strain, failure energy and peak modulus) compared to the untreated fibril.[22] Previous studies performed on collagen fibrils using AFM nanoindentation (see section 3.4.1) showed that the radial indentation moduli are in the range of 1-12 GPa in air, while

values of 0.5-200 MPa are reported in the wet state, which resemble the physiological environment. [12]
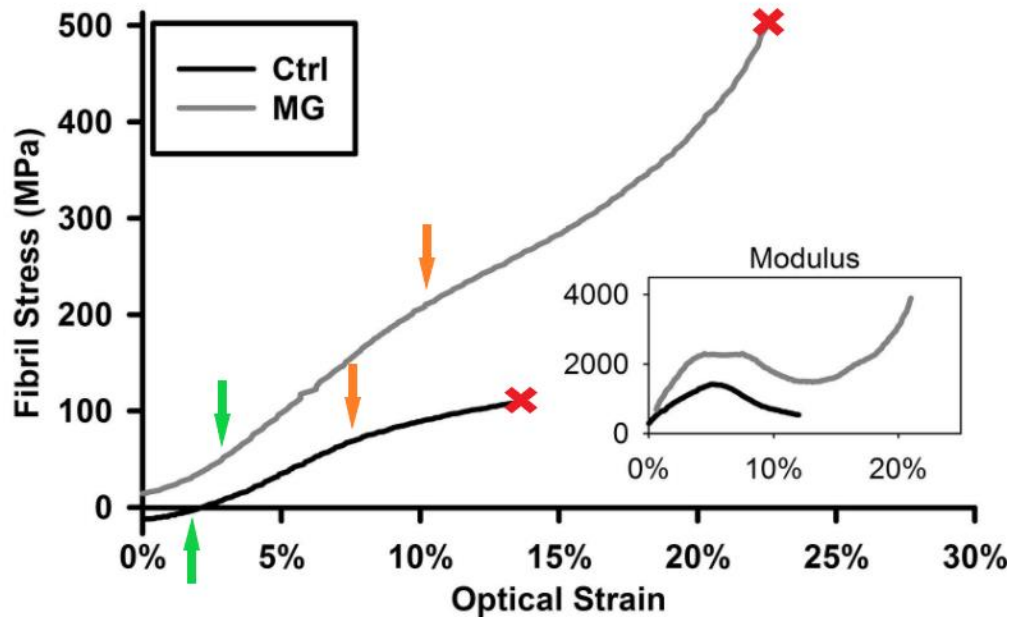
Figure 8: The stress-strain curves of nano tensile test on collagen fibril of a mouse-tail tendon, black curve represents the untreated fibril, while the grey one is a glycated fibril with MGO [22]

Viscoelasticity

The mechanical behavior of materials can be examined by measuring the relation between stress and strain while applying external loading. It can be generally classified as elastic, plastic, or viscoelastic behavior as shown in Figure 9. Elastic materials have no hysteresis in the force-distance curves as the loading and the unloading curves coincide. Plastic behavior occurs during loading and leads to permanent deformation of the material.[15]
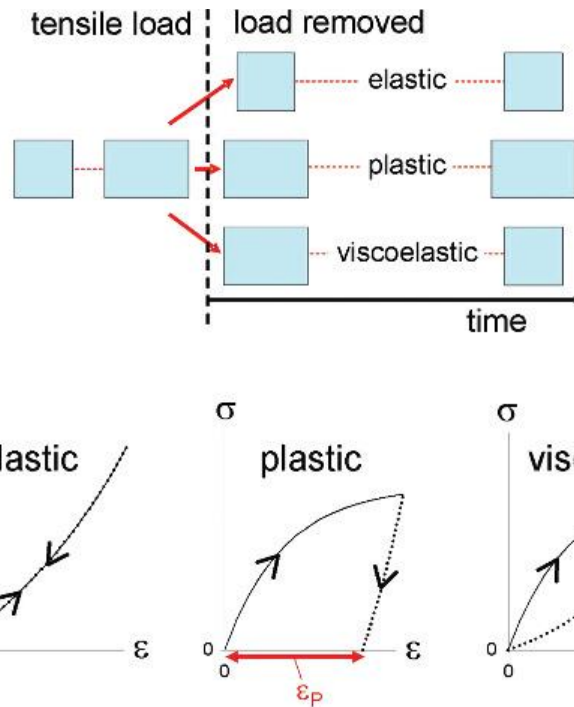
Figure 9:   the different mechanical behavior of materials after loading and unloading of a tensile load (top), the stress-strain curves of the elastic, plastic and viscoelastic materials are shown (bottom), where σ is the stress and ε is the strain [6]

Viscoelastic materials have a distinctive property, that is, the relationship between stress and strain is not constant but changing depending on the rate of change.[15, 23] This can be observed through the dependence of the effective stiffness on the rate of the application of the force. Hysteresis in approach and retract curve due to energy dissipation, creep, stress relaxation and phase lag are phenomena that occur in experiments during cyclic loading on viscoelastic materials.[5]

The earliest mechanical characterization experiments showed that biological materials have remarkable properties that cannot be fully described as purely elastic materials. The behavior of these materials compiles both solid and liquid aspects, which can be described as viscoelastic.[5] Although collagenous tissues are known to be viscoelastic, the sources of this viscoelasticity and the way the forces are transferred from the lower hierarchical levels to the higher ones are not completely understood.[24]

The important role of viscoelasticity was demonstrated at all levels of hierarchical structure. While the cause of this viscoelastic behavior could be a result to the complex structure of these biological materials as they are composed of solid and fluid components. The existence

of the hierarchical structure, the active dynamics and force generation is thought to explain this behavior too. Experiments in the time and frequency domains with special methods are required to reveal the viscoelastic properties of these materials.[5]

As biological materials are generally soft, exhibiting values of apparent modulus ranging from 10s of Pa to several MPa, the investigation of the small scales in the hierarchical structure demands forces and displacements at the micro- and nanoscale. Development of the biomechanical instruments such as micropipette aspiration, optical/magnetic tweezers, stretchers, cell traction force microscopy, atomic force microscopy (AFM) and nanoindentation are necessary to overcome this challenge and enable investigating the samples in an aqueous environment.

AFM dynamic oscillatory nanoindentation testing (see section 3.4.2) at a range of physiologically relevant frequencies (i.e., walking, breathing, heart cycle is approximately at 1 Hz) reveals the microrheological properties of biological tissues, which is of great importance in particular cells like epithelial cells in lung, which is subjected to large cyclic forces due to breathing. [9]

3 Atomic Force Microscopy (AFM)

Since the invention and the commercial appearance of the AFM it has become an important instrument for probing different materials and biological tissues in particular. It is a method for imaging the topography of a surface in three-dimensional detail down to the nanometer scale. Images of different materials, hard or soft, synthetic or natural such as cells and biomolecules can be acquired in air, liquid or in some cases under vacuum. Unlike light or electron microscopes, AFM images the sample surface using a sharp tip known as a probe. The tip is attached to a flexible microcantilever, which bends under the influence of force, as it acts as a simple spring with spring constant K.[25]

AFM methods offer a variety of tools for assessing the micromechanical properties of materials by measuring the interactions between the microcantilever probe and the sample surface.[5]

3.1 AFM Principle

As mentioned before, AFM uses a cantilever with a very sharp tip to scan over a sample surface. While the tip approaches the surface and atomic distances are reached, an interaction between the particles of the tip and the sample known as the Lennard-Jones (L-J) potential is present. It includes the long-range attractive Van der Waals forces and the short-range repulsion forces and can be described as:

$$w(r) = 4\varepsilon \left[\left(\frac{\sigma}{r}\right)^{12} - \left(\frac{\sigma}{r}\right)^{6}\right] = -\frac{A}{r^6} + \frac{B}{r^{12}} \qquad (3.1)$$

where ε is the depth of the local minimum of the potential energy, σ [m] is the distance at which the Lennard-Jones potential is zero and r [m] is the distance between particles. A and B are the attractive and repulsive components respectively. Figure 10 shows the Lennard-Jones potential as a function of the distance between the particles of the tip and the sample. At the very right-hand side of the figure, the tip is far away from the sample surface and there is no interaction between the tip and the surface of the sample. At closer range, the Van der Waals attractive forces between the tip and the surface emerge and cause a deflection of the cantilever towards the surface. When the cantilever gets even closer to the surface, the short-range electron shell repulsive forces take over and cause the cantilever to deflect away from

the surface.[13, 15, 26] Imaging in liquid environment in case of biological samples reduces the Van der Waals forces and is less destructive to the delicate samples, thus minimizes damage compared to imaging in air. As the tip is fully submerged in liquid and the tip-sample distance approaches molecular dimensions, other forces come into play and become significant. Solvation forces appear due to the interaction between the solvent molecules and the surfaces of both tip and sample and lead to oscillations in the force detected. This oscillatory force profile arises from the repeated ordering and disordering of the liquid molecules as adequate pressure between the two surfaces is reached. These unique forces influence the friction, wear, lubrication, and adhesion properties of the samples. Steric forces are also short-range forces appear in liquids due to the high affinity for interacting with liquid rather than the solid surface.[27, 28]

$$w(r) = -\frac{A}{r^6} + \frac{B}{r^{12}}$$

$$A = 4 \cdot \epsilon \cdot \sigma^6, B = 4 \cdot \epsilon \cdot \sigma^{12}$$
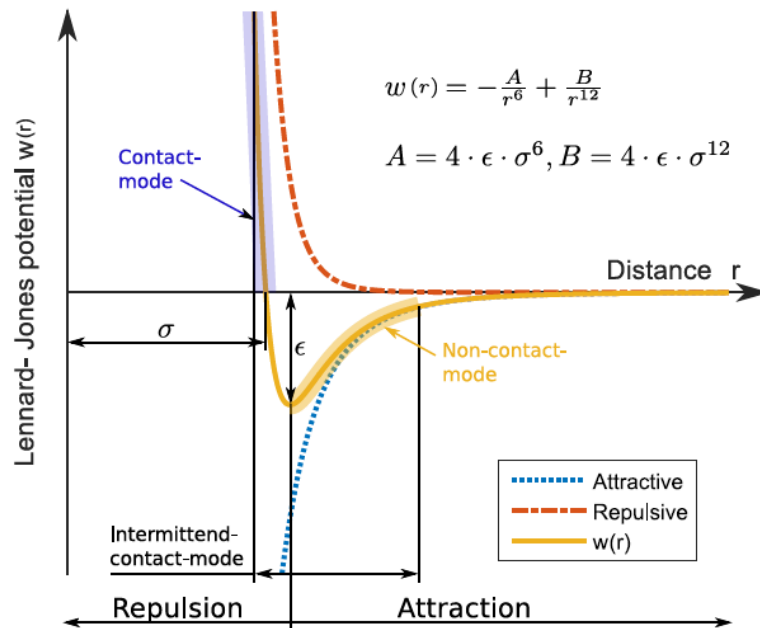
Figure 10: the yellow curve shows the Lennard-Jones potential, with the attractive Van der Waals forces (the blue dotted line) and the short-range electron shell repulsion forces (the red dot dashed line). ε is the depth of the local minimum of the potential energy [29]

The electrostatic force is an important long-range force, which is present at the solid-liquid interface due to the electrical charge developed on the solid surface. In electrolyte solutions

most surfaces and adsorbed biomolecules develop a surface charge and are surrounded by ions of opposite sign. Due to the arrangement of the electric charge around the surface and the balancing charge in the solution an electrical double layer (EDL) is formed. In AFM, when the surface of the tip and the sample surface approach each other, an interaction appears due to the overlapping of the EDL of both surfaces and consequently an electrostatic force builds up. EDL interactions play a crucial role in case of biological systems due to their long-range character, to the physiological medium containing concentration of ions, and to the substantial charge of molecules such as amino and nucleic acids.[27]

The deflection of the cantilever is measured using different detection methods like interferometry, capacitive sensors, piezoresistive/piezoelectric sensors and the optical lever method. In most current AFMs, the optical lever method is the commonly used method, where a laser beam is reflected from the microcantilever and detected by a quadrant photodiode as seen in Figure 11. The collected voltage signal is then amplified and processed by a digital signal processor (DSP). The measured deflection is related through the cantilever's spring constant K to the force between the sample and the cantilever.[12] Figure12 shows the force distance curve including the approach and retract curves.
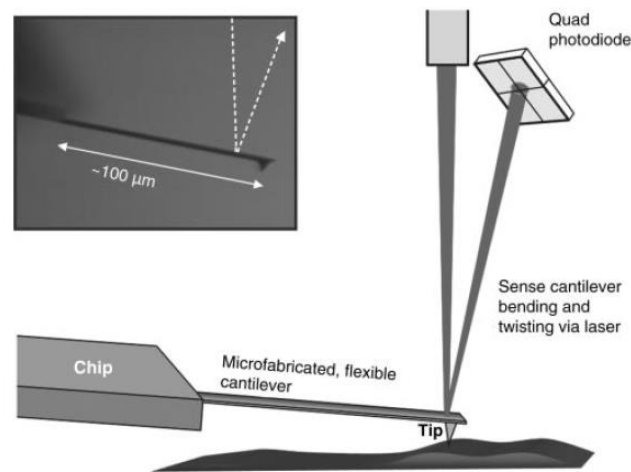
Figure 11: the cantilever with the tip propping the sample surface and reflected laser beam on the photodiode can be seen in this figure [25]
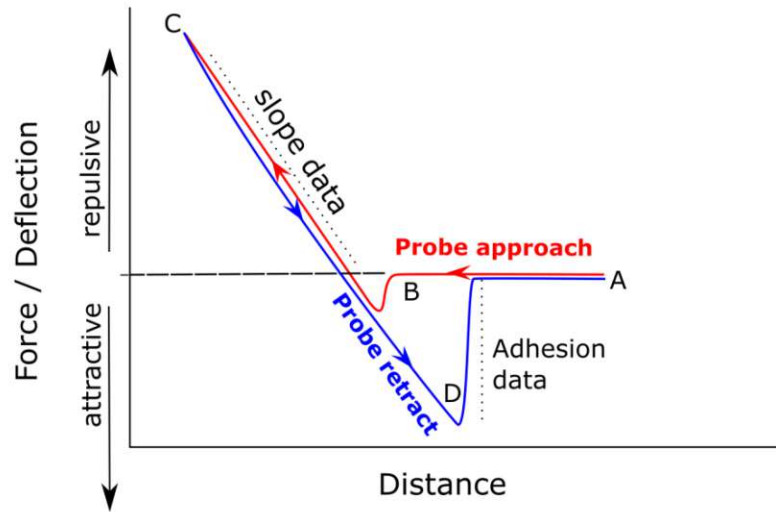
Figure 12: force-distance curve due to cantilever tip approach and retract to the sample surface [30]

A piezoelectric actuator permits the probe movement in a three-dimensional manner relative to the sample and hence scanning and indentation experiments can be performed.[5]

In the recent years many AFM techniques have been developed to explore biological samples. The flexibility of AFM comes from the ability to control and measure force (stress) and indentation (strain) precisely leading to implementing a large selection of experimental protocols. Moreover, AFM provides a high spatial resolution mapping of the viscoelastic behavior of the biological samples.[5]

3.2   Feedback loop

The feedback loop is a control loop that maintains the predefined set point constant, which resembles either the deflection or the oscillation amplitude of the cantilever while imaging. In response to that the movement of the piezoelectric actuator, which drive the cantilever position relative to the sample surface, can be adjusted.

For AFM devices three control types are commonly used, the proportional, the integral and the Derivative (PID) controller. The proportional control amplifies the error, which is the difference between the actual value and the setpoint and then generates a correction signal. It reacts quickly to changes on the sample surface. However, proportional control leads to an offset value (actual value is slightly higher or lower than the setpoint). With the help of the

second control, which is the integral part the introduced offset can be removed as it helps to reach the accurate value of the setpoint. The derivative controller is then added, which results in a homogenous signal by reducing the unwanted oscillations. Figure 13 shows a block diagram of the PID controller principle and Figure 14 illustrates how the PID controller works.[15]
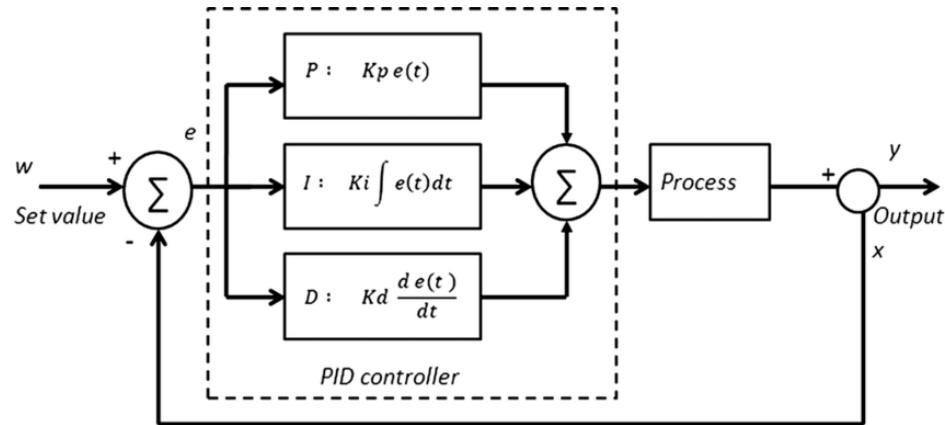
Figure 13: block diagram of the PID controller, showing the three control parts : the proportional, the integral and the Derivative [31]
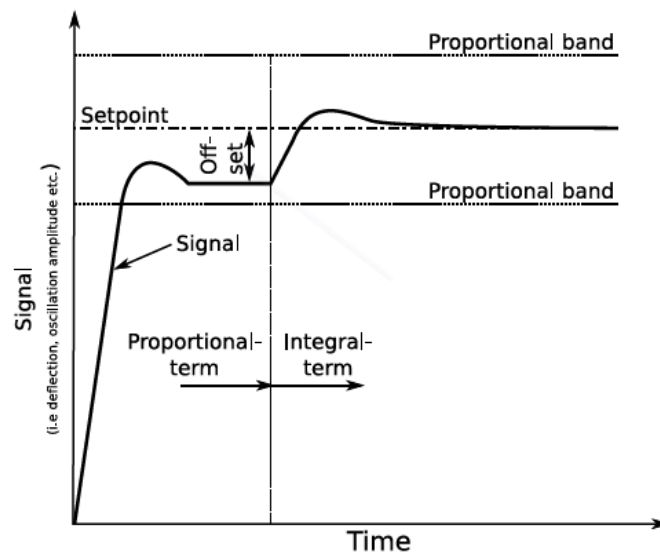
Figure 14: the work of the PID controller on the deflection/oscillation signal [32]

3.3   Imaging modes

The AFM cantilever is scanned over the surface of the sample in all imaging modes.[13] The classification of the imaging modes is related to the cantilever tip oscillation during imaging and hence there are two basic modes of imaging: static or contact mode and dynamic mode.[33] The dynamic mode can be further divided into tapping or intermittent contact mode and non-contact mode. The different modes have different distances between the AFM cantilever tip and the sample surface as can be seen in Figure 15. There are two fundamental dynamic modes, amplitude modulated AFM (AM-AFM) and frequency modulated AFM (FM-AFM).[25]

3.3.1 Contact mode

Contact mode is the simplest and the oldest used AFM imaging mode, where the tip is brought into contact with the surface of the sample while scanning across the sample.[33]

Two types to obtain images in this mode, either constant height or constant deflection (force). In case of constant height, the changes in the deflection of the cantilever derive the surface topography. This type of imaging mode has several drawbacks as it causes damage of the sample and the tip due to the continues contact. A better approach is the constant deflection, where a feedback loop aims to maintain constant cantilever deflection and consequently a constant interaction force.[13]

3.3.2 Non-contact mode

This dynamic AFM mode gives the opportunity to image the sample without having a direct contact to its surface, offering lowest possible interaction between the tip and the sample, and hence preventing both the tip and the sample from being damaged. The AFM cantilever oscillates near its resonance frequency with a smaller amplitude (1 nm or less) than in AC tapping mode, where the tip is kept at distance of several nanometers away from the sample surface. The disadvantage of this mode is that it is challenging to keep the AFM tip in the attractive regime.[13, 34]

3.3.3 AC Tapping mode

Also called intermittent mode, similar to the non-contact mode the cantilever oscillates by a piezoelectric actuator close to its resonance frequency, usually several tens to several hundred kilohertz with a certain amplitude near the surface. This mode overcomes the problem of lateral forces, which appears in contact mode.[13, 34]
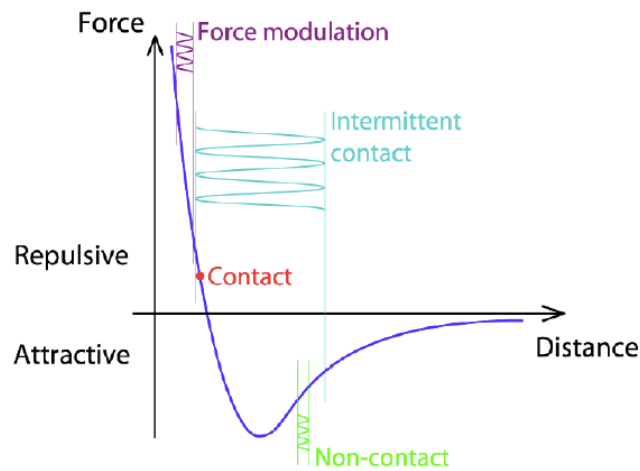
Figure 15: the different imaging modes, with the force between the tip and the sample surface [15]

3.3.4 QI mode

The quantitative imaging mode (QI mode) is a very robust and stable imaging mode. It collects force-distance curves at every pixel in a high-resolution image hence this mode is a fast-imaging mode with high resolution imaging in every environment especially fluids. It has a great performance for soft, sticky and loosely attached samples, so it is a perfect mode for cells and tissues. This mode has several advantages over the conventional imaging modes: it is a non-destructive measurement compared to contact mode due to zero lateral forces, which preserve the sample and the tip. In case of conventional AC mode, the sample can be compressed due to non-directly controllable vertical forces, while in QI mode low forces down to 10 pN can be reached, which ensures the lowest tip-sample interaction and prevents both sample and tip from damage. With QI mode there is no need to adjust the set point or optimize the gain. Qi mode does not need a complicated feedback loop as in the

previous above-mentioned modes, it needs just a threshold deflection to trigger the retract.[13, 35]

3.4 Additional AFM techniques

These AFM techniques are based on one of the aforementioned basic imaging modes, allowing investigating a variety of other sample properties.[34]

3.4.1 Force volume mapping

Studying the viscoelastic properties of nano-systems has made nanoindentation methods extremely important in the last few decades as they focus on the micro and nano scale, which is crucial to understand biomechanics of living cells and their response to external forces. Nanoindentation with AFM is one of the most important and popular methods. The conventional AFM force-distance curves are used to extract the important properties of the materials, such as elastic modulus, stiffness, and adhesion using mainly two fitting models, which are Hertz and Oliver-Pharr models.[36] This mode is a quasistatic mode where it is a series of nanoindentation in a grid-like pattern. The tip is pressed into the sample vertically just on the grid points, and while moving from point to point there is no contact between the tip and the sample. It is similar to the QI imaging mode, with the difference that nanoindentation is slower and the loading rate is lower while the main focus is on the mechanical properties and not on the topology of the sample.[12]

3.4.2 Dynamic nanoindentation

Dynamic nanoindentation also referred to as microrheology, has become a multifunctional and powerful method for many applications for the purpose of the detection of micro-nanoscale force, viscoelastic properties, and other physical properties. It is a useful technique that reveals information about the mechanical properties of materials with nonuniform mechanical properties. Dynamic nanoindentation is a natural extension of the previous technique, where the viscoelastic properties can be measured at each point by adding an oscillation into each force curve. Despite the large benefits of this technique, such as the high spatial resolution it has a shortcoming that is the low acquisition speed, which can be up to

several hours. This is due to the application of multiple periods of oscillations recorded at the selected frequencies, which leads to high acquisition time for the low frequencies. The low excitation frequencies take long periods of time, which leads to the high acquisition time. In this dynamic method the cantilever vibrates far from its fundamental flexural resonance. While moving in a grid like pattern in contact mode, a periodic signal with a small amplitude compared to the indentation amplitude, mechanically drives the AFM cantilever in the vertical direction to probe the frequency dependent response of the surface. The oscillations are applied to the Z-direction to push directly on the sample surface, while the vertical cantilever deflection signal is monitored as shown in Figure 16. In case of hard surfaces like glass for example, the whole oscillation is transferred to cantilever deflection and there is no damping in the amplitude of the applied signal. On soft surfaces such as biological materials the tip sinks into the soft surface and hence the measured amplitude of the cantilever deflection is smaller than the applied oscillation (see Figure 17).

There is also a phase shift between the applied signal and the monitored signal, both the amplitude and the phase of these two signals give the storage and loss modulus.[5, 25, 37, 38]
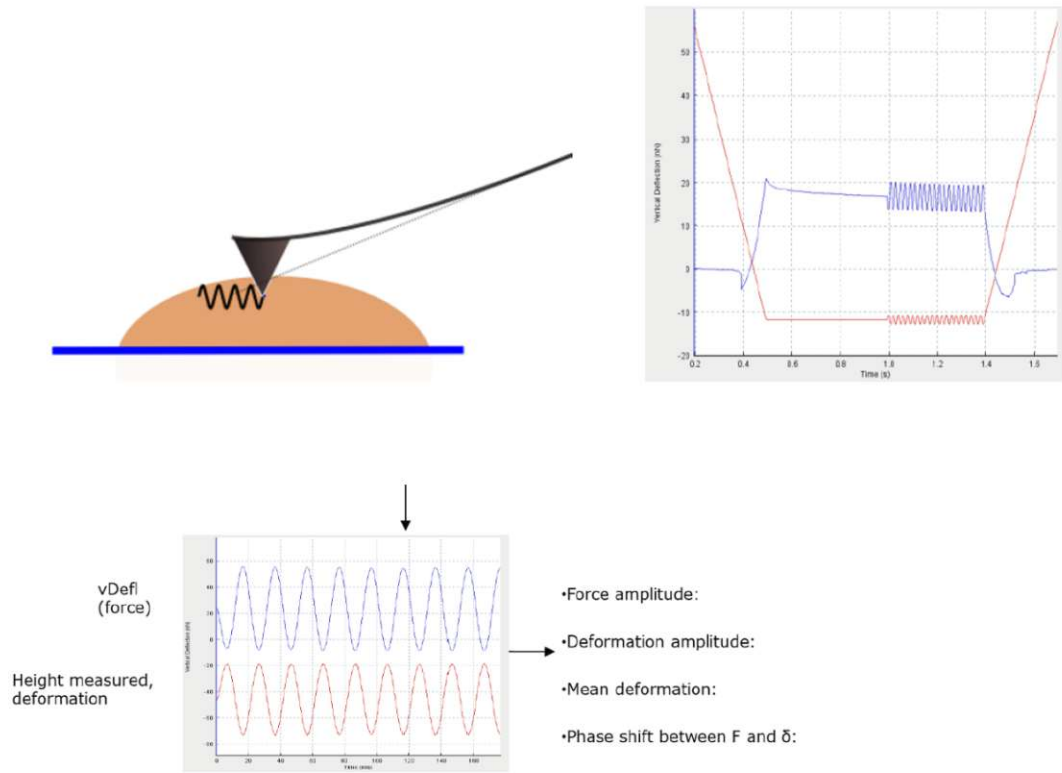
Figure 16: on the top left, the cantilever oscillating while in contact with the sample, where the height and the measured deflection signals are shown on the right [37]

The indentation can in general be described as a sine function of time,

$$\delta(t) = \delta_0 + \delta_A \sin \omega t \tag{3.2}$$

which is occurring around an operating indentation depth δ_0, $\delta_A \ll \delta_0$, where the force F(t) has both sine and cosine components,

$$F(t) = F_0 + F' \sin \omega t + F'' \cos \omega t \tag{3.3}$$

The complex modulus of the material is then

$$E^*(\omega) = E'(\omega) + iE''(\omega) \tag{3.4}$$

where $i = \sqrt{(-1)}$, $E'(\omega)$ is the elastic (storage) modulus of the material and is proportional to the in-phase component of the frequency-dependent indentation. $E''(\omega)$ is the viscous (loss) modulus and is proportional to the out-of-phase component.

In case of an elastic material (solid), the force is exactly in phase with the input deformation and $E''(\omega) = 0$, while in case of a viscous material (liquid), the induced stress is out of phase with the input deformation and $E'(\omega) = 0$.

The loss tangent $E''(\omega)/E'(\omega)$ is an important index of the solid-like or liquid-like behavior as it gives the ratio of the viscous and elastic stiffness.

The complex modulus in case of biological materials like tissues and cells, shows a marked dependency on the frequency of the strain. Multi-frequency signals that are composed of several sine waves or a sweep signal in which frequency increases with time can be applied. These frequencies are much lower than the resonance frequency of the microcantilever and hence the analysis is simplified. [5]
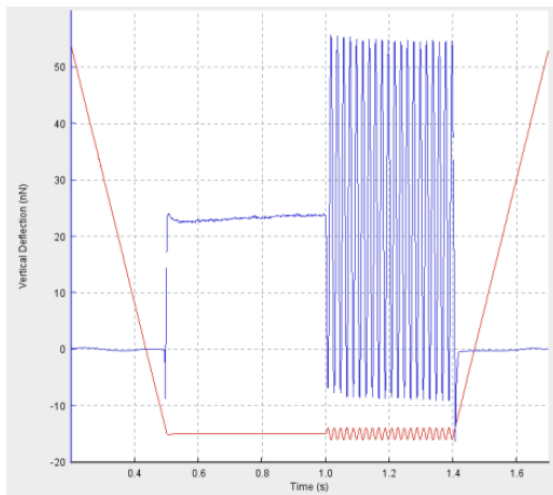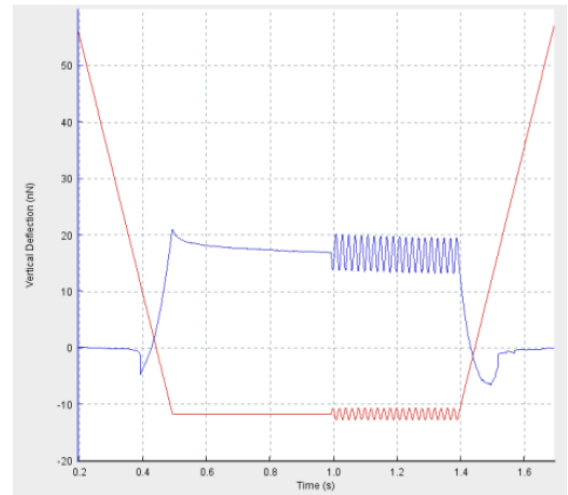
Figure 17: the difference between indentation on hard and soft surfaces, to the left the stiff surface where there is no damping in the force signal, while on the right the force signal is damped due to the soft tissue. [37]

Tensile testing

Other than AFM, Tensile testing is an important widely used tests. Data resulting from tensile tests (relates displacement and sustained force of the material) are further processed to be independent of the sample geometry, which gives then the stress-strain diagrams. Through stress-strain diagrams different materials can be compared as these diagrams are independent

of the geometrical parameters of the samples. Tensile testing gives important information about the mechanical properties of the collagen fibrils. This is achieved through testing them in their natural loading case, which is tension. Several research groups have performed tensile tests on collagen fibrils in different ways with various instruments. Among the different experiments, three methods developed to perform tensile tests on collagen fibrils are worth mentioning. Microelectromechanical Systems (MEMS) [39], Micro-manipulators [10] and Atomic force microscope [40]. Nonetheless, these methods have shown some downsides, for example AFM needs a lot of adjustment and is time consuming, while the Microelectromechanical Systems (MEMS) provides inferior resolution and bandwidth compared to other instruments.[15]

In the present work a novel instrument introduced by Nalbach et al. (see section 4.2.2) is used to examine fibrils with quick sample coupling and uncoupling. This instrument provides tensile testing at minimum bandwidth of 1 KHz with force resolution (p-p) of 10 nN and strain resolution of 0.1%.[41]

Dynamic mechanical analysis (DMA)

Dynamic mechanical analysis is a powerful and commonly used technique that measures the viscoelastic behavior of materials. It measures the response of the sample to an oscillating load. The phase lag between the applied stress and the measured strain indicates the material's tendency to flow (viscosity), while the sample recovery indicates the material's stiffness (modulus). Different from traditional tensile testing, DMA provides a modulus value for each sinusoidal stress cycle. Through DMA a complex modulus is obtained, which is different than the modulus obtained from the linear region of the classical stress-strain curve. Complex modulus reveals the elastic modulus, which indicates the ability to store energy, and the loss modulus, which exposes the tendency for viscous energy loss.[42]

4 Materials and Methods

4.1 Sample Preparation for indentation

A skinned tail of a 14 week-old wild type (WT) mouse stored at -80 ˚C (to prevent tissues from degradation) was used for the preparation of the samples used in this thesis. Collagen fibrils were extracted from the tail tendon by cutting a small piece of tissue (a few millimeters) in the longitudinal direction from a tendon fascicle. It was then transferred to a microscope slide (VWR® Microscope Slides) and kept hydrated using a few drops of deionized water for easier further manipulation. A small piece of this fascial tissue (< 1 mm) containing the collagen fibrils was then pulled out and spread on another slide under a low magnification stereomicroscope (SZX10, Olympus, Japan) using a pair of fine tweezers. The slide was then rinsed with deionized water to get rid of minerals and unwanted tissue debris. Then, it was dried in air and kept in a closed box letting the fibrils adhere to the slide. The dry samples were investigated with optical microscopy to locate single separate collagen fibrils.

For this thesis, a control and a test group were prepared containing ten fibrils each. Both groups were harvested from the same mouse tail and the same fascicle.

4.1.1 Additional sample preparation for tensile testing

Isolated and intact fibrils aligned orthogonally to the long axis of the microscope slide were chosen (ten fibrils on each slide). For the dynamic tensile test, an additional preparation on these fibrils was performed. A magnetic bead of 30- 50 µm in diameter, made of neodymium alloy (product number: MQP-S-11-9-20001, Magnequench International LLC, China) was attached to the collagen fibril using epoxy resin (two component epoxy resin, UHU plus end fest 2-K_Epoxidharzkleber, UHU, Germany) under an inverted light microscope (model: 139 IX73, Olympus, Japan) using a custom-made magnetic tweezer and by applying a magnetic field. The resin was prepared by mixing continuously, for 5 minutes the same amount of the two components of the epoxy with the spatula. On the other end of the fibril a small droplet of the epoxy resin was placed on a distance of approximately 100 µm to the

glued bead (to be able to conduct the tensile test without hindering the microgripper) using an ultra- fine tungsten probe [41]. The fibrils were then left for at least 24 hours to let the resin cure. Figure 18 shows the prepared collagen fibrils with the beads and the resin droplet.
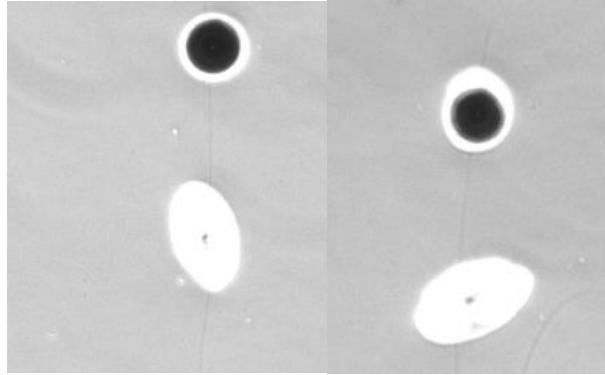
Figure 18: fibrils with the attached bead and the epoxy droplet, aligned orthogonally to the side of the microscopic slide

A rectangular fluid cell with an area of 3.0 mm x 2.5 mm and a height of 0.5 mm was mounted on the slide using a two-component silicon adhesive, on the area enclosing the smeared fibrils as in shown Figure 19. It is important to be able to examine the fibrils in a physiological environment using a physiological salt solution such as phosphate buffered saline (PBS).
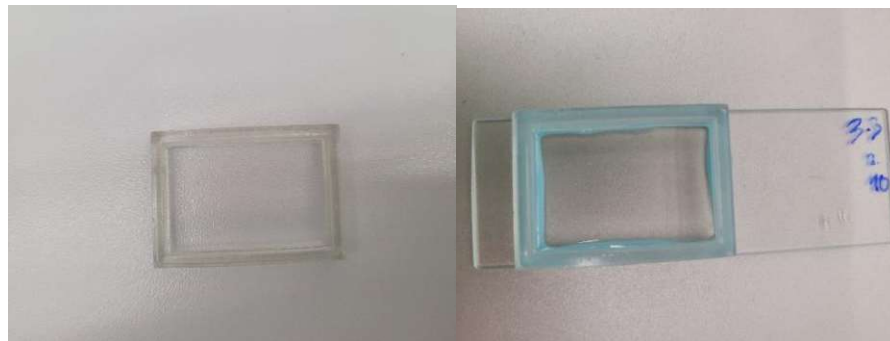
Figure 19: a fluid cell with the dimensions of 3 mm x 2.5 mm x 0.5mm is mounted on the microscope slide to be filled with PBS to examine the fibrils in a physiological environment

4.1.2 MGO and control buffer solutions

For the preparation of the MGO group, which is the test group mimicking the cross-links in collagen fibrils in case of aged and diabetic patients, one of the two slides prepared was used as the test group. The fibrils on this slide were incubated in an MGO solution in the temperature-controlled incubation chamber at a temperature of 34°C for four hours. Then the

samples were rinsed with distilled water, left to dry in air at room temperature and then kept in a clean box until the measurement day.

A buffer of MGO solution containing 20 mM/L of MGO (Methylglyoxal), 5 mM/L of EDTA (Ethylenediaminetetraacetic Acid) and 10 mM/L of PBS (Phosphate Buffered Saline) was prepared. A few drops of NaOH (Sodium hydroxide) were added at the end to the solution to increase its pH value to 8 to avoid denaturation of the fibrils during incubation.

For the control group a buffer solution containing 10 mM/L of PBS (Phosphate Buffered Saline) and 5 mM/L of EDTA (Ethylenediaminetetraacetic Acid) was prepared.

4.2   Experimental workflow and study design

Two experiments were performed on both slides on the same fibrils to explore their viscoelastic properties and to examine the effect of glycation on their behavior. These were dynamic nanoindentation using AFM and dynamic tensile tests using a new testing device introduced by Nalbach et al., termed NanoTens.[41] Figure 20 shows the study design of this thesis.

As most of the fibrils on the control slide ruptured before measurement with the NanoTens device in the second part of the experiment. An additional control sample slide was needed and supplemented with fibrils from the same fascicle for data completeness.

```
┌─────────────────────────────────┐
│          Study design           │
└─────────────────────────────────┘
┌─────────────────────────────────┐
│       Sample preparation        │
└─────────────────────────────────┘
┌──────────────────┐   ┌──────────────────┐
│  Control group   │   │    Test group    │
└──────────────────┘   └──────────────────┘
┌─────────────────────────────────┐
│      AFM basic indentation      │
│      AFM force modulation       │
└─────────────────────────────────┘
┌──────────────────────┐   ┌──────────────────┐
│ Incubation in        │   │ Incubation in MGO│
│ control solution     │   │                  │
└──────────────────────┘   └──────────────────┘
┌─────────────────────────────────┐
│      AFM basic indentation      │
│      AFM force modulation       │
│      Dynamic tensile test       │
└─────────────────────────────────┘
┌─────────────────────────────────┐
│          Data analysis          │
└─────────────────────────────────┘
```
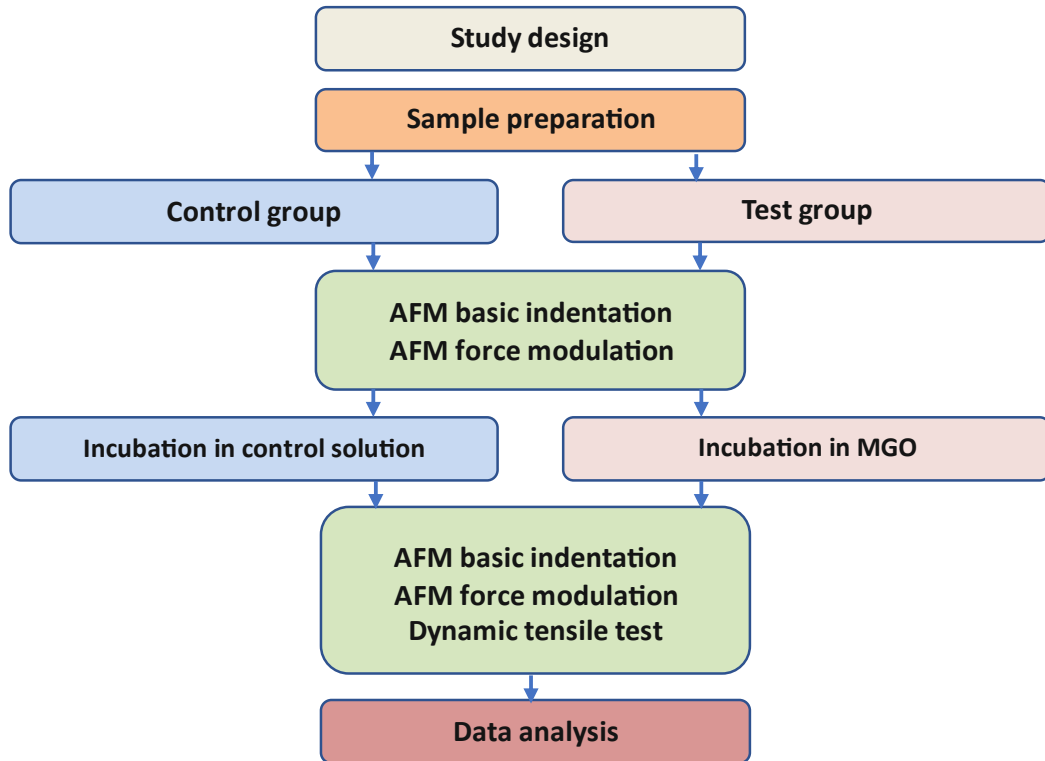
Figure 20: the study design of this master thesis, where two methods were used, one with AFM dynamic nanoindentation and the other dynamic tensile test

4.2.1 AFM force modulation method:

For this method, an AFM workstation with a JPK Nanowizard Ultra Speed A (Bruker Crop., Billerica, MA, USA) [12] was used, which is mounted on a Zeiss Axiovert (Carl Zeiss AG, Oberkochen, Germany) [12] inverted microscope.

The cantilever used for all the measurements is a Nano World PNP-DB cantilever (NanoWorld AG, Neuchatel, Switzerland) [12]. The tip of the cantilever has a pyramid shape, and is one of four cantilevers mounted on a chip, where on each side of the chip two different cantilever sizes can be found.

The probe used in this experiment is cantilever A, with dimensions of 100 μm x 40 μm x 0.5 μm, nominal stiffness of 0.48 N/m and resonance frequency of 67 kHz. A measurement of a TGT1 sample with the used AFM cantilever was performed before measuring. This is done by scanning the TGT-1 grating in contact mode, which is a known surface, to get information about the real shape of the used cantilever tip. Through this information the contact area (A_c) can be defined, which is needed for the indentation measurements. Calibration of the

cantilever in air was done using the AFM software directly before each measurement and after the laser alignment, where the stiffness of the cantilever was determined using the Sader method, provided in the JPK software. In this method the spring constant of the cantilever is calculated knowing the quality factor Q_f of the surrounding medium (» 1 in case of air), the length l, the width w and the resonance frequency w_f of the cantilever through the following relation:

$$k = 0.1906 \, \rho_f \, w^2 \, l Q_f \, \Gamma_i \, (w_f) \, {w_f}^2 \qquad\qquad (4.1)$$

where k [N/m] is the spring constant, w [Hz] is the oscillation frequency, l [m] is the cantilever length, ρ_f [kg/m^3] is the density of the fluid (air, liquid), Γ_i is the imaginary component of the hydrodynamic function, which depends on the Reynolds number and w_f is the resonance frequency.[13] Through the fitted model of the thermal noise spectrum implemented in the JPK software, the resonance frequency w_f and the spring constant k can be determined.
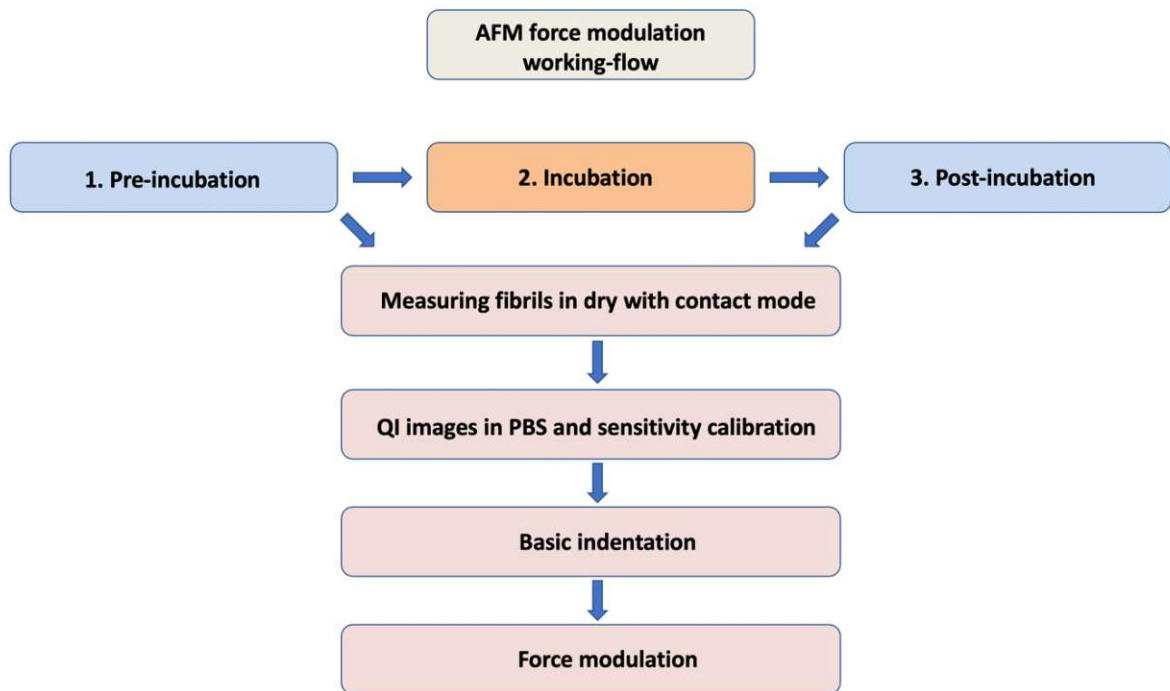
Figure 21: the workflow of the first method, in which both groups are measured pre- and post- incubation with the protocol showed in the scheme.

The workflow of this method on each fibril on both slides (control and test) is shown in Figure 21, where the following steps were performed on fibrils pre- and post-incubation. The incubation step was done on each slide in the relevant buffer for four hours in the incubation chamber at 34° C.

First, the chosen fibril was imaged in dry state to make sure it is intact, showing D-banding, and it is just a single fibril with a height in the normal range (50 to 300 nm). This was done with imaging in contact mode, by choosing a 2 µm x 2 µm area including the fibril with a resolution of 512 x 512 pixels. I Gain was set to 120 Hz, P Gain to 0.001 and the set point to 1.0 nN.

To indent the fibrils in a physiological environment a fluid cell was mounted on the sample slide, and the cell was filled with a 0.25 ml PBS (Phosphate-buffered saline) solution.

After a waiting period of 30 min, to ensure thermal equilibrium, a QI image of the same fibril was taken, with a set point of 2 V, Z-length of 500 nm, pixel time of 50 ms and pixel size of 128 x 128.

On a clean spot on the glass near the imaged fibril, a small area of 100 nm x 100 nm was then chosen to perform the sensitivity calibration of the cantilever, using force mapping in contact mode. This was done by looking at the 25 deflection curves of the glass spot near the fibril and by taking the slope of the head height-vs-deflection curve as the inverse optical lever sensitivity. This was done with the assumption that the stiffness of the cantilever is orders of magnitude lower than the stiffness of the glass, which means that the indentation depth on glass is negligible. After the sensitivity calibration, fibril nanoindentation was then performed using basic force mapping in contact mode with a grid of 1.0 µm x 1.5 µm size, 64 x 16 pixels and with a pixel ratio of 4:1 where the fibril is centered in the middle of the grid and perpendicular to the imaging fast axis.

Following the basic indentation an advanced dynamic oscillatory indentation was carried out at the same fibril at a range of physiologically relevant frequencies, using the force ramp designer in the advanced force mapping in contact mode (see Figure 22). A 1.5 µm x 1.5 µm window including the fibril is chosen with 16 x 1 pixels, to have enough pixels on the fibril to be able to catch the apex of the fibril. Eleven segments of the ramp designer were chosen, starting with approach segment, and ending with retract segment.
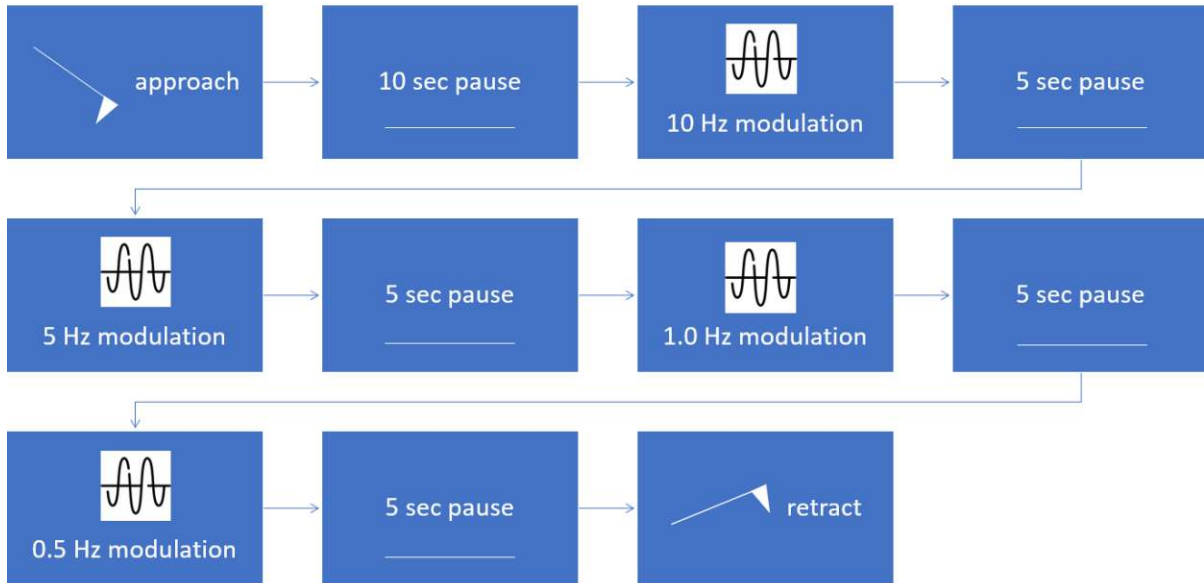
Figure 22: the 11 segments chosen in the force ramp designer, starting with the approach segment followed by a long pause of 10 s then the modulation segments and pauses, and ending with the retract segment

A frequency sweep with frequencies of 0.5, 1.0, 5.0 and 10 Hz was applied in a decreasing order of frequency to avoid excessive creep accumulation, as can be seen in Figure 23. Four height-controlled pauses (each with 5 seconds) in between the four segments and before the retract segment were chosen, while a longer height-controlled pause (10 seconds) after the approach segment was applied to reduce the creep (see Figure 23).
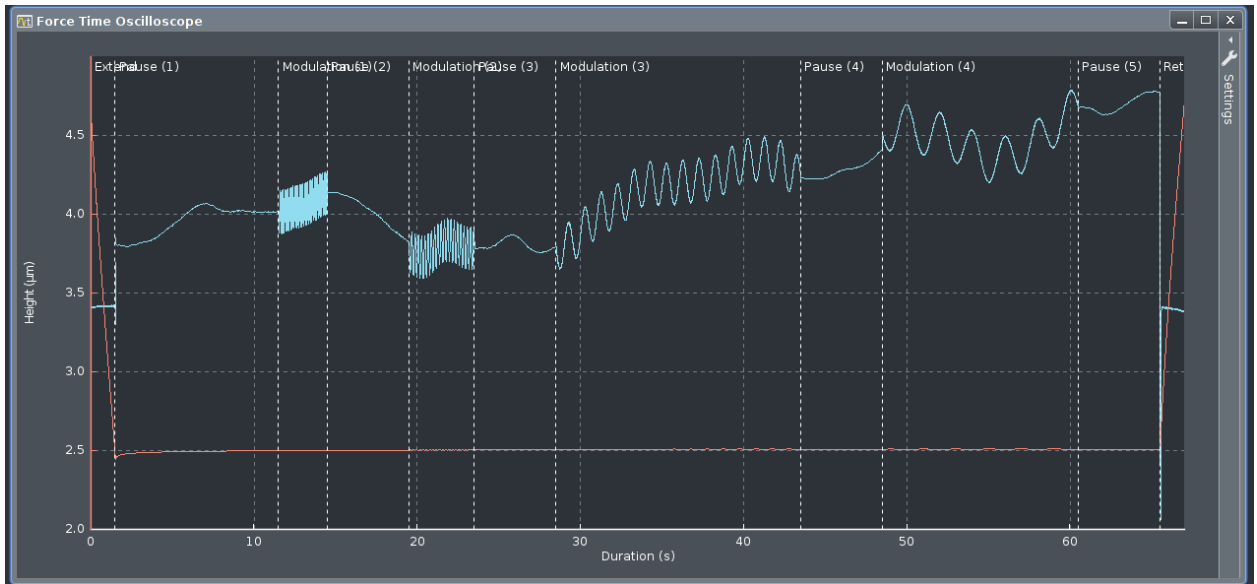
Figure 23: the frequency sweep applied on the fibril, where red is the height signal, and blue is the deflection signal, the frequencies were applied in a decreasing order to reduce excessive creep accumulation

A set point of 1.0 nN and an indentation amplitude of 2.0 nm was used. One cycle of indentation takes about 1 min and the whole measurement of 16 pixels of one fibril takes about 18 minutes. Figure 24 shows the 16 x 1 pixels image with five pixels showing the fibril including the fibril apex.

The aforementioned protocol was conducted on each of the ten fibrils on both control and MGO group (slide) before and after incubation in the relevant buffers.
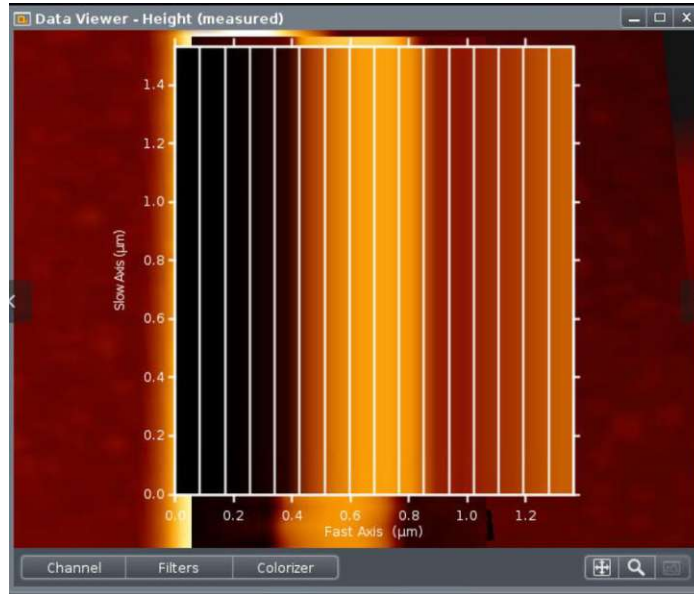
Figure 24: the 16x1 pixel image, where 5 segments located on the fibril and the rest are on the glass

4.2.2 Dynamic Tensile Testing:

Following the force modulation measurements on the AFM, dynamic tensile tests were performed on each individual collagen fibril using a novel tensile testing instrument developed by Nalbach et al., termed NanoTens.[41] Figure 25 shows the different parts of the instrument. A fiberoptic cantilever probe (Optics 11, Netherlands), which is partially submerged into aqueous solution (PBS) is mounted on a piezo lever actuator. The cantilever deflection due to fibril loading, results in an interference signal, which is measured by the OP 1550 interferometer. The piezo lever actuator is mounted on a stepper motor translation stage. The deflection of the cantilever and the position of the piezo lever actuator are acquired with a CompactRIO controller (National Instruments, USA).
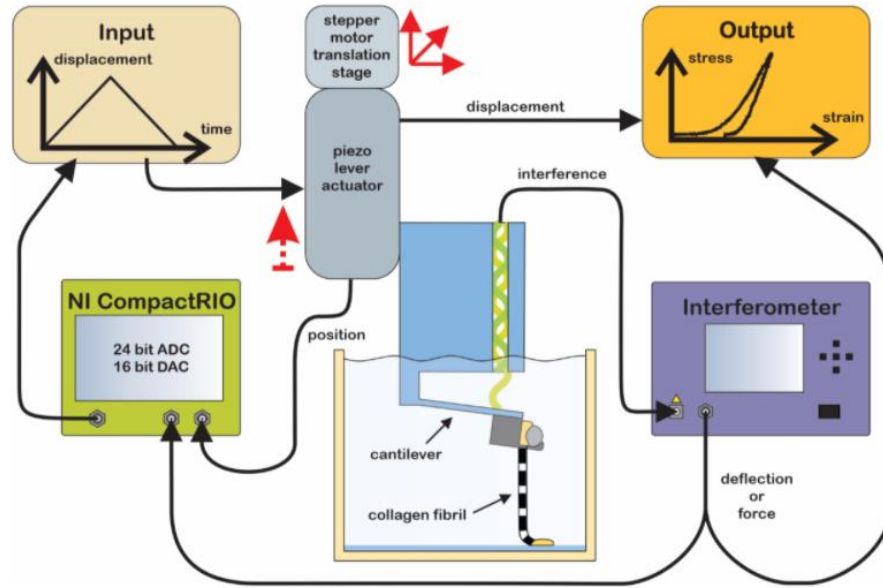
Figure 25: Shows a schematic of the NanoTens instrument. The different parts of the instrument can be seen, the interferometric force probe mounted on a piezo lever actuator is partially submerged into PBS, the cantilever with the microgripper where the fibril with the magnetic bead is placed and the acquisition unit, which is a CompactRio controller.

The tensile test was performed under a light microscope with fibrils contained whitin a fluid cell filled with PBS. The chosen fibril was cut behind the magnetic bead and gently the bead with the fibril was detached from the microscope slide using ultra-fine tungsten probe. After the calibration of the interferometric force probe, the magnetic bead along with the fibril was lifted by applying a current to the magnetic tweezer and approaching the bead. The collagen fibril with the bead was then picked up by a 3D-printed microgripper attached to the cantilever tip of the interferometric force probe.

To conduct a dynamic tensile test, the piezo lever actuator was used to load the fibril in the desired loading pattern. In this work a frequency sweep of 0.05, 0.1, 0.5 and 1.0 Hz, with force setpoint of 1 µ N and 2 µN, and an amplitude of 200 nN were applied on each measured fibril. After loading the bead with the fibril into the microgripper, the force set point was adjusted to 1 µN and the controller I gain was tuned to be able to reach the set point quickly. The DMA protocol started with an initial holding time of 30 s at a force set point of 1 µN, followed by the four signals at the selected frequencies separated by 10 s pauses between each frequency signal. The same protocol was repeated at a force set point of 2 µN, then a

tensile test in open loop mode with 5% /s strain rate was conducted on the fibril until it ruptured.

In case of testing without fibril rupture, the magnetic tweezer is activated again with maximum current and approached to the magnetic bead with the fibril, where the bead was then picked up from the microgripper. Figure 26 shows the pick-up of the fibril through the bead with the microgripper and the detachment process.
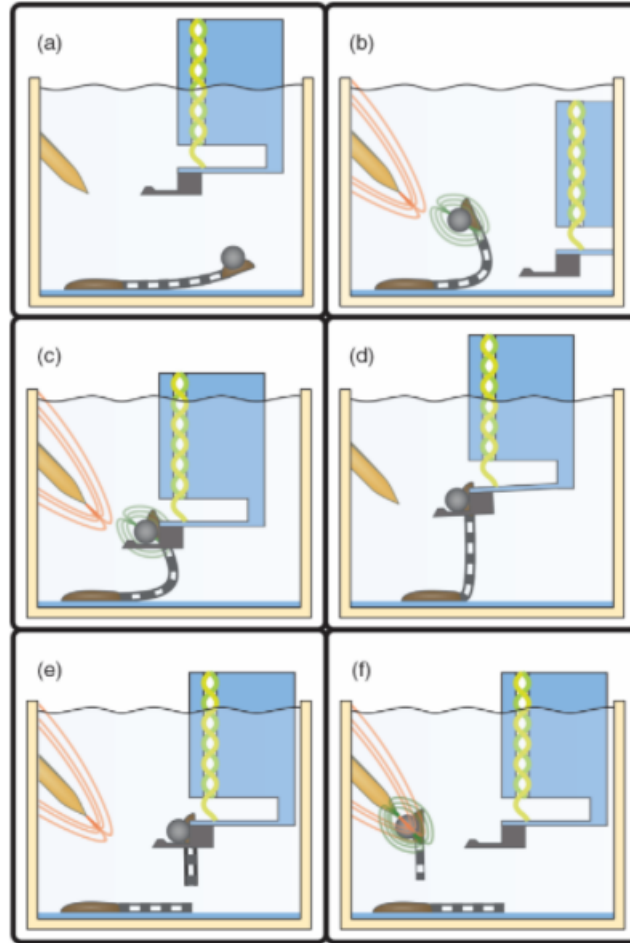
Figure 26: a drawing of the pick-up and the detachment process, (a) Shows the magnetic tweezer, the microgripper and the collagen fibril with the magnetic bead. (b) The magnetic tweezer approaches the bead after activation, causing lifting of the fibril. (c) Picking up the magnetic bead. (d) Placing the bead into the microgripper, the collagen fibril is aligned with the z-axis and the tensile test can be performed. (e) After testing the fibril to failure, the magnetic tweezer is activated again and approaches the bead on the fibril. (f) Unloading the bead with the rest of the fibril from the microgripper.

5 Results

5.1 AFM Dynamic nanoindentation results

It was aimed to collect data from 10 fibrils on each slide of the two experiment groups. 13 fibrils were prepared on each microscope slide, but not all of them could be measured as some fibrils were not oriented properly, leading to difficulties through measurements. For AFM dynamic nanoindentation, 10 fibrils on each slide could be measured. The individual collagen fibrils of both groups: control and MGO, were measured before and after incubation in the relevant solutions with the specified protocol described in the method section (see section 4.2.1). The chosen four frequencies were physiologically relevant. However, the very low frequencies (0.1 and 0.2 Hz), which were designed firstly to be investigated, were avoided in AFM measurements due to high noise in indentation and force signals causing problems with signal fitting and data analysis. Figure 27 shows the fitted indentation and the fitted resulting force signals on glass, where it is clear, that there is no damping in the indentation signal as expected for hard surfaces. While Figure 28 shows the indentation signal on the fibril with the damped force signal with a slight phase shift as expected for soft tissues.
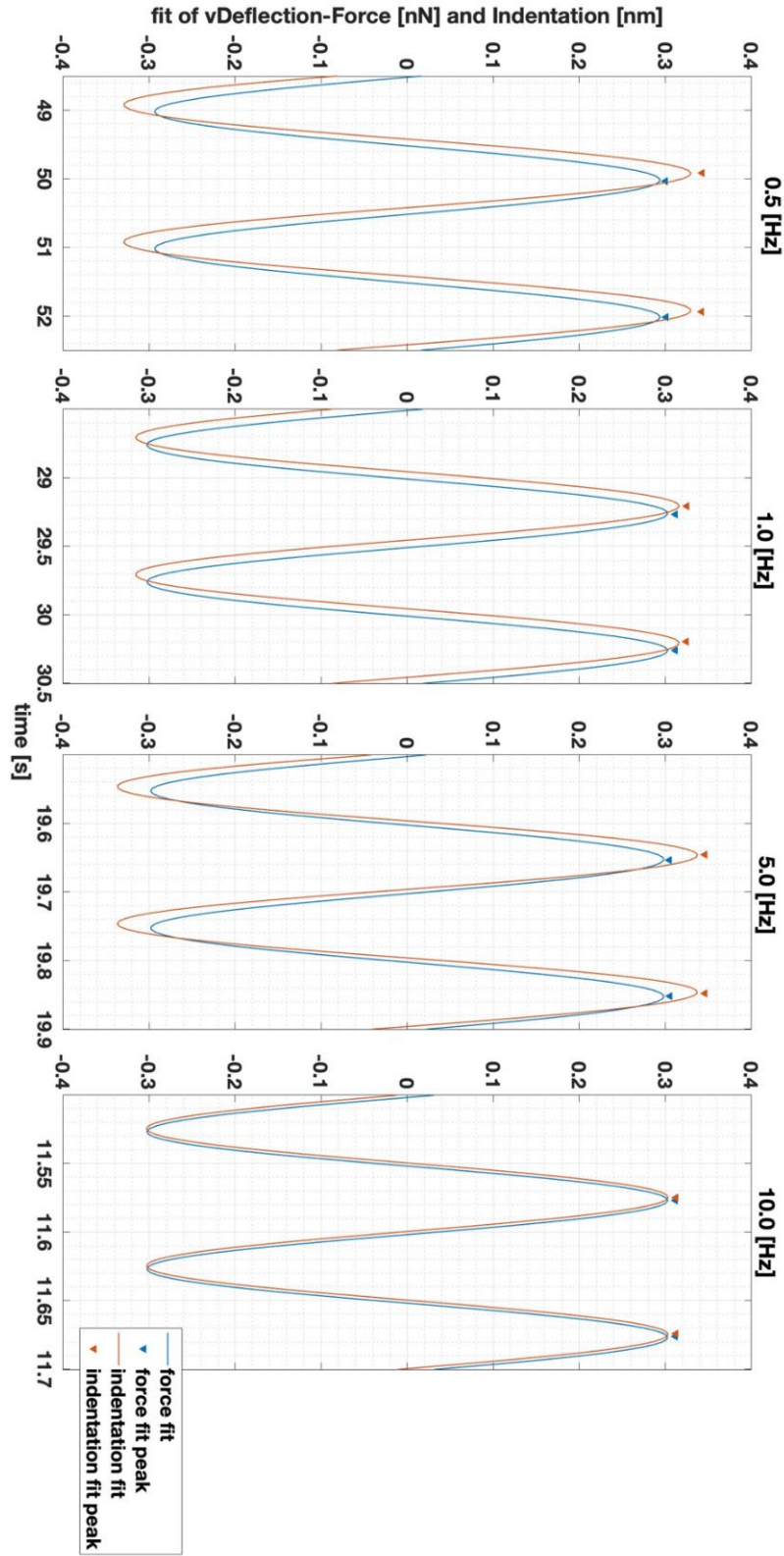
Figure 27: the fitted force and indentation signals on glass over the selected four frequencies, showing no damping in the force signal as the indentation is on a hard surface
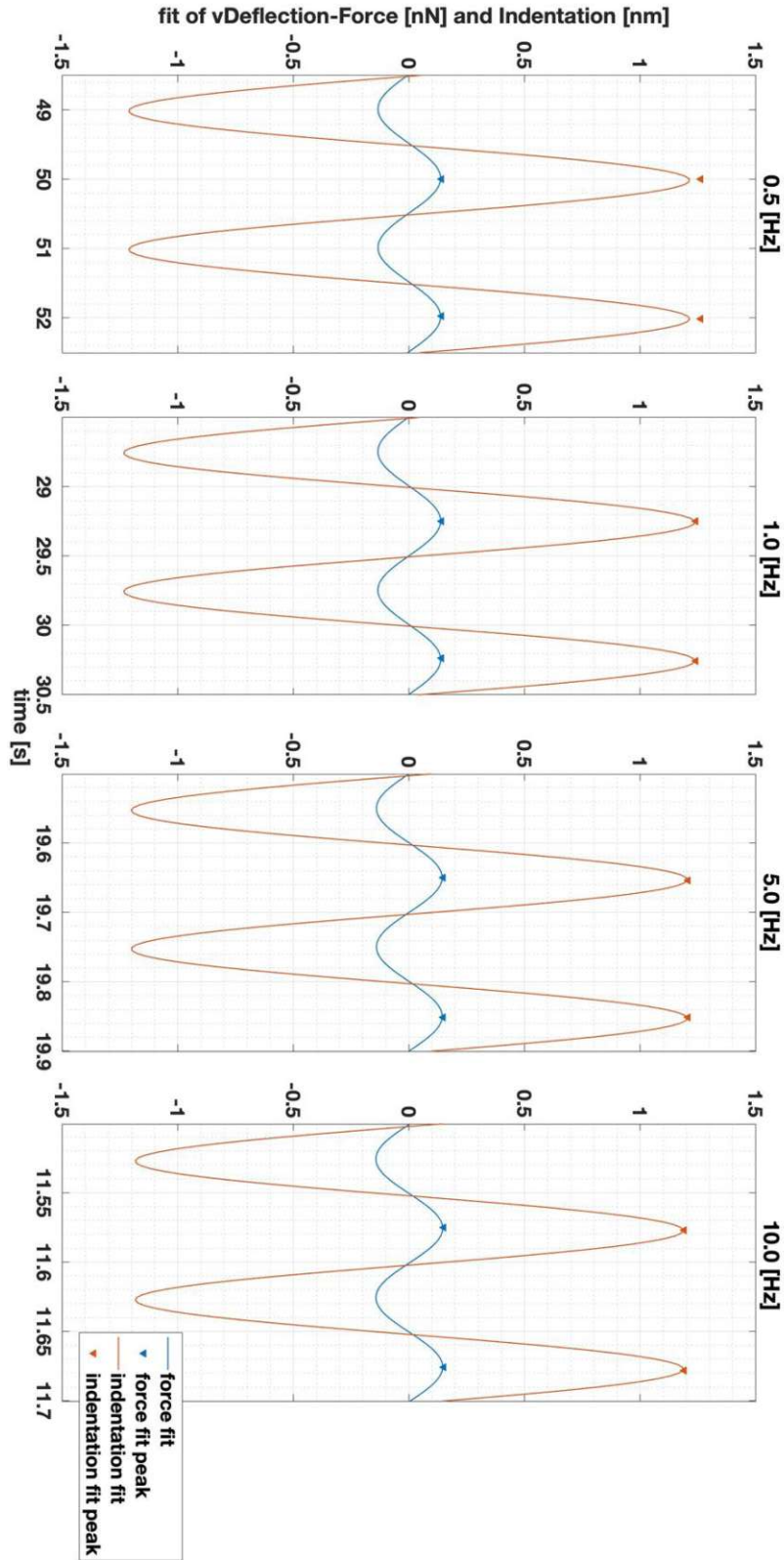
Figure 28: the fitted force and indentation signals of one of the fibrils of the control group, showing the damped force signal due to the soft material.

All the analyzed data were collected from nine fibrils on each slide, as one fibril (on each slide) was avoided due to noisy indentation and force signals, which resulted in bad quality data, especially of the DZ-slope. This is mainly due to the high drift during the measurement of these two fibrils. The data points on each fibril were chosen looking at different parameters like the DZ-slope values, which is less than one in case of soft tissue (around one for glass), the phase shift, as it is a few degrees for the soft tissues, the resulted damped force signal on the fibril. The apex point is the highest point on the fibril having the same height value as the fibril diameter. Figure 29 (a) shows a mask of one of the fibrils with the apex point indicated on the fibril, where in figure 29 (b) the DZ- slope values of the 16 pixels are shown with 5 pixels on the fibril (8-12). In figure 29 (c) the diameter of the fibril can be seen, as well as the index of the apex point and the apex height. The phase shift values in degrees between the indentation and force signals can be seen in Figure 30, where it is just a few degrees for the pixels on the fibril.
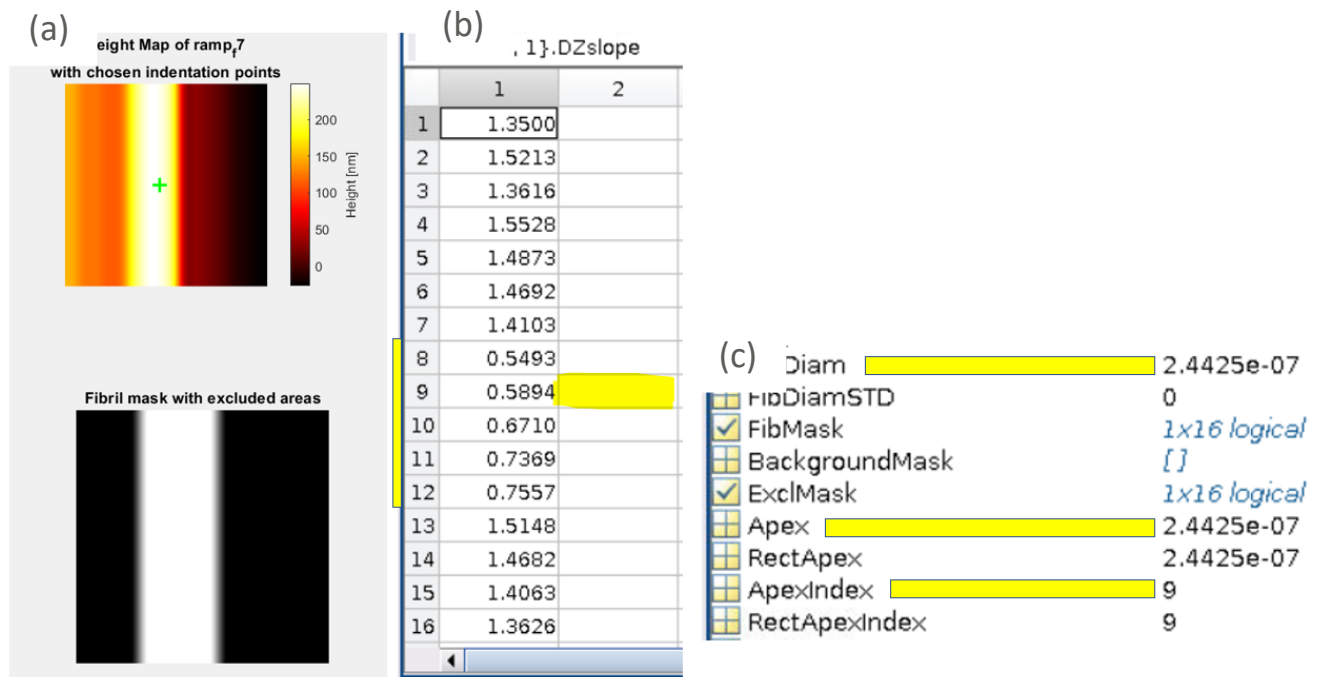
Figure 29: showing a random fibril from the control group pre incubation, (a) shows the fibril mask and the selected indentation point on the apex of the fibril (the green cross), (b) show the DZ-slope values on the 16 pixels with the yellow line showing the 5 pixels on the fibril, (c) shows the fibril diameter and the apex height.

E.FM{1, 1}.DeltaPhi								
1	2	3	4	5	6	7	8	9
[]	[]	178.4711	[]	-180.2279	[]	-180.2035	[]	174.4110
[]	[]	179.2109	[]	-181.1730	[]	179.5806	[]	181.2231
[]	[]	178.1971	[]	-180.4772	[]	-180.3013	[]	178.6543
[]	[]	177.5462	[]	-180.7875	[]	-179.8256	[]	178.2417
[]	[]	179.0271	[]	-181.0898	[]	178.9252	[]	173.4815
[]	[]	178.0977	[]	163.5966	[]	178.9347	[]	179.9282
[]	[]	177.1016	[]	161.4599	[]	174.4566	[]	182.2723
[]	[]	5.6919	[]	5.1849	[]	4.5206	[]	3.4098
[]		5.8439	[]	6.1196	[]	4.8672	[]	3.5010
[]	[]	7.5795	[]	6.0622	[]	2.8511	[]	10.4862
[]	[]	5.3787	[]	6.2722	[]	6.5672	[]	8.0034
[]	[]	8.0094	[]	10.7007	[]	10.9635	[]	7.9659
[]	[]	179.3542	[]	-180.1219	[]	-179.7509	[]	179.6412
[]	[]	179.0585	[]	-180.3706	[]	-180.2360	[]	179.9102
[]	[]	179.1321	[]	-180.1381	[]	-180.2615	[]	182.1284
[]	[]	179.3751	[]	-180.3553	[]	179.2295	[]	177.7671

Figure 30: the phase shift in degrees between the indentation signal and the force signal for all the 16 pixels, with the pixels on the fibril (8-12) with just a few degrees.

For the data from the 9 fibrils of each group before and after incubation, the mean values ± the standard deviation of the loss tangent, the storage modulus, the loss modulus and the dynamic modulus were calculated. The change in these parameters before and after incubation in the control as well as in the MGO group were tested statistically using a paired T-test.

Table 1. shows the mean values of the loss tangent of 9 fibrils from each group over the four defined frequencies. To examine the viscoelastic behavior of the fibrils, the changes in the loss tangent values were evaluated at the selected frequencies. A significant increase ($P < 0.003$) in the loss tangent from 1.0 Hz to 5 Hz was observed in the control group before incubation, as well as after incubation from 1.0 Hz to 5 Hz ($P < 0.05$) and from 5 Hz to 10 Hz ($P < 0.01$). For the MGO group, the mean value of the loss tangent increased significantly ($P < 0.002$) with frequency from 5 Hz to 10 Hz before glycation. The loss tangent of all groups except the MGO group after treatment, showed a dependency on frequency.

Comparing the loss tangent of the control group before and after incubation to detect the effect of incubation on fibrils, no difference was detected after incubation whereas in the

MGO group a significant increase (P < 0.04) after glycation could be detected at 1.0 Hz. The boxplots of the mean values of the loss tangent calculated at the four frequencies for both groups before and after incubation can be seen in Figure 31.

Table 1:   the mean values of the loss tangent ± the standard deviation of 9 fibrils in each group at four frequencies, for both control and test group before and after incubation in the relevant solutions. A significant increase is observed at 1.0 Hz for the MGO group after glycation (P < 0.04)

Loss Tangent (Mean value)				
Frequency [Hz]	0.5	1.0	5.0	10
Control group pre-incubation N = 9	0.104 ± 0.088	0.071 ± 0.025	0.098 ± 0.014	0.098 ± 0.022
Control group post-incubation N = 9	0.086 ± 0.056	0.074 ± 0.039	0.086 ± 0.029	0.109 ± 0.040
MGO group pre-incubation N = 9	0.055 ± 0.036	0.048 ± 0.015	0.056 ± 0.014	0.073 ± 0.014
MGO group post-incubation N = 9	0.086 ± 0.065	0.071 ± 0.032	0.072 ± 0.043	0.075 ± 0.037
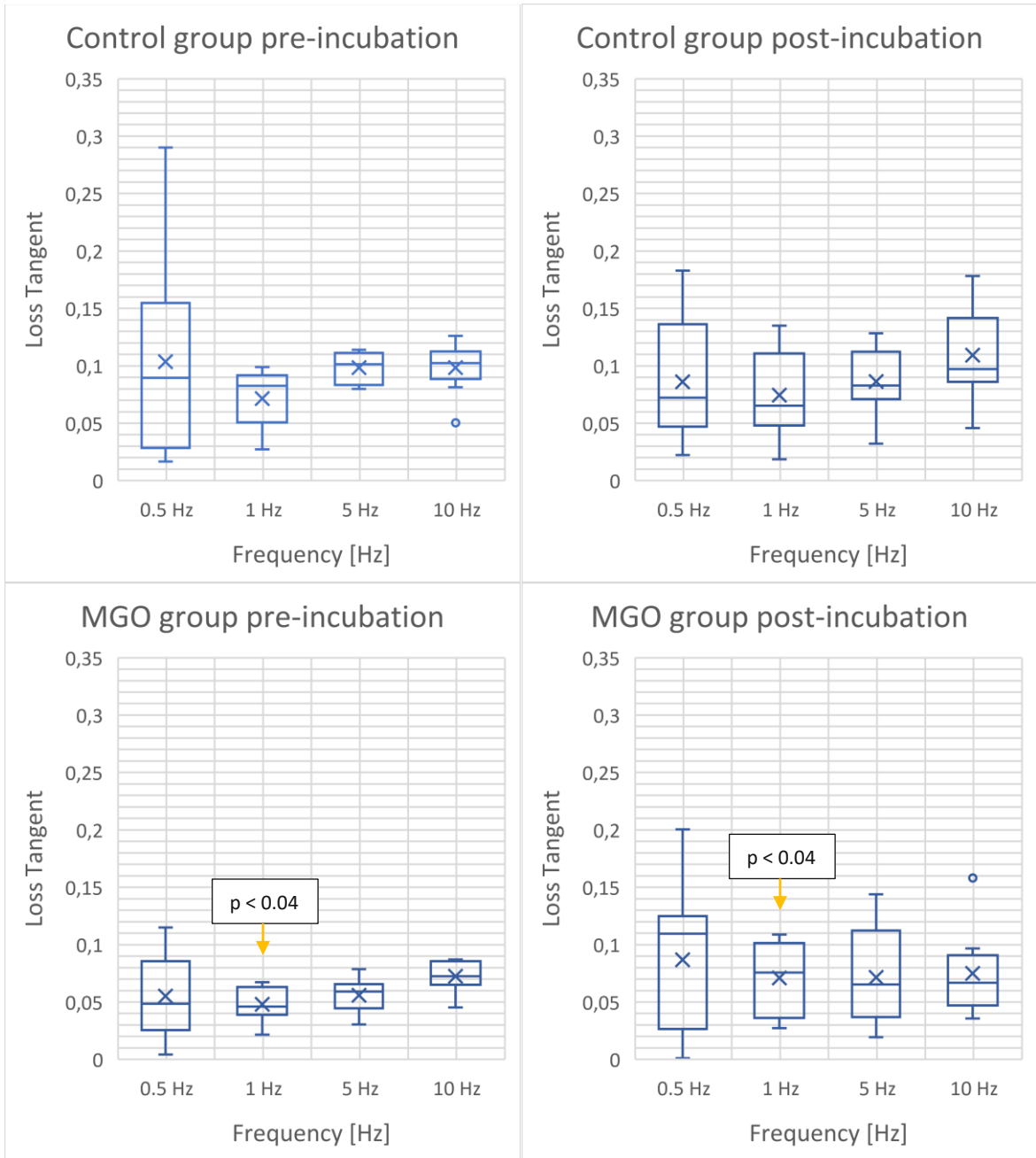
Figure 31: Boxplots of the mean values of the loss tangent of the control and MGO groups before and after incubation. The central line of each box shows the median, while the bottom and top edges of the box show the 25th and the 75th percentile respectively. The two whiskers show the max (top) and min (bottom) values. The crosses in the boxplots show the mean values, and the small circles show outliers.

Table 2. shows the mean values ± the standard deviation of the storage modulus of 9 fibrils from each group at the selected four frequencies. Comparing the mean values of the storage

modulus over frequency, they showed a significant increase going from 1 Hz to 5 Hz in control group after incubation ($P < 0.03$). Whereas in the MGO group before incubation there was significant decrease ($P < 0.03$) from 1 Hz to 5 Hz. Again, the fibrils of the MGO group did not show any change with changing frequency.

Looking at the fibrils of the same group before and after incubation, only a significant increase ($P < 0.05$) in the storage modulus in the control group was detected at 10 Hz. The boxplots in Figure 32 show the mean values of the storage modulus for both groups over the selected four frequencies

Table 2: shows the mean ± the standard deviation values of the storage modulus in MPa of 9 fibrils for both control and test group before and after incubation in the relevant solutions, with a significant increase ($P< 0.05$) at 10 Hz for the control group after incubation.

Storage modulus (Mean value) [MPa]				
Frequency [Hz]	0.5	1.0	5.0	10
Control group pre-incubation N = 9	1.437 ± 0.79	1.345 ± 0.63	1.409 ± 0.67	1.384 ± 0.59
Control group post-incubation N = 9	1.509 ± 0.61	1.519 ± 0.61	1.656 ± 0.69	1.623 ± 0.63
MGO group pre-incubation N = 9	2.189 ± 0.73	2.015 ± 0.58	1.879 ± 0.51	1.894 ± 0.58
MGO group post-incubation N = 9	2.282 ± 0.96	2.014 ± 0.76	2.10 ± 0.66	2.073 ± 0.83
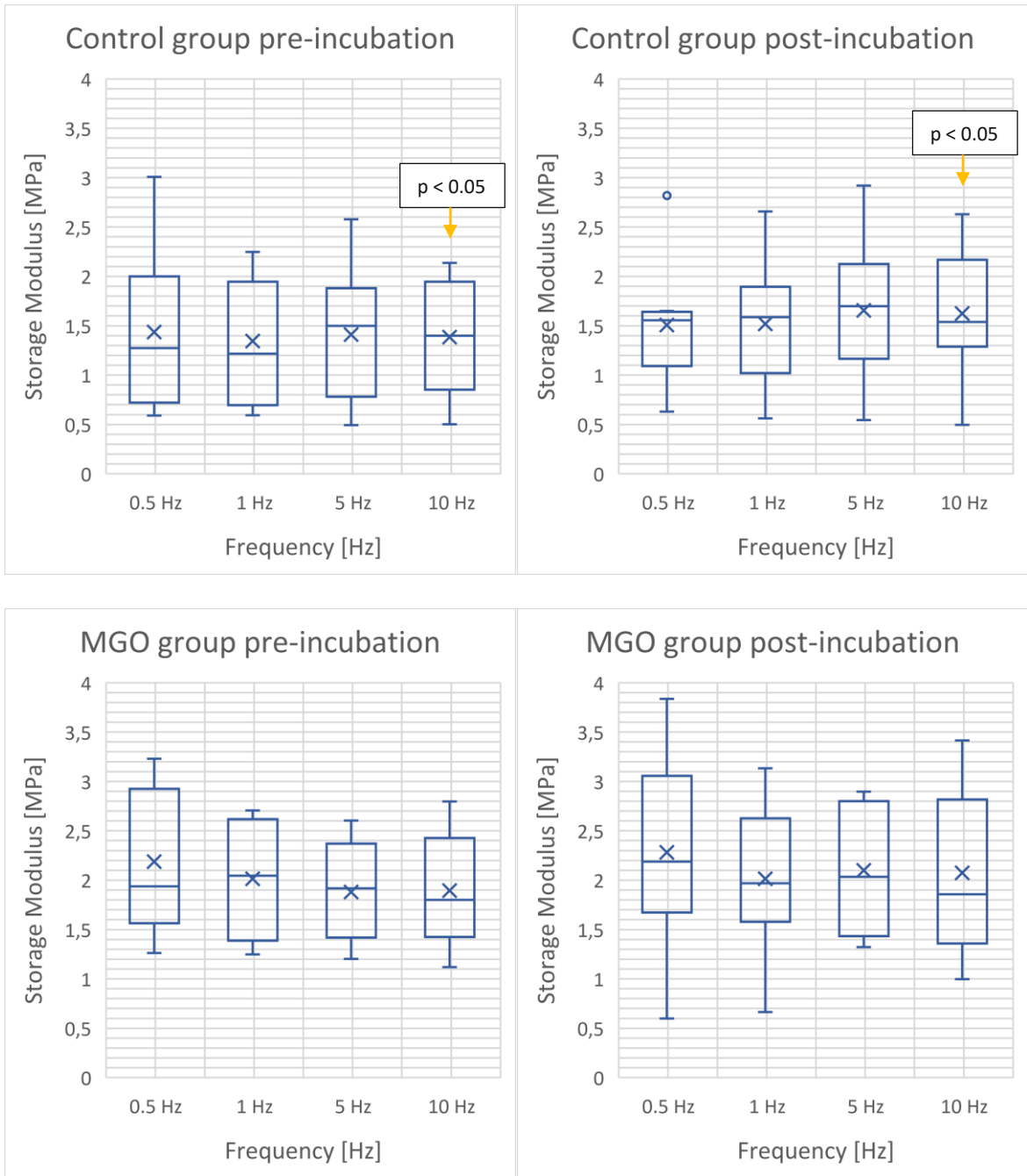
Figure 32: Boxplots of the mean values of the storage modulus in MPa, of 9 fibrils for both control and test group before and after incubation.

The mean values of the loss modulus of the 9 fibrils from each group are shown in table 3. Looking at the behavior of the loss modulus over frequency, a significant increase ($P < 0.003$) from 1.0 Hz to 5 Hz in the control group before incubation was detected. Whereas for the control group after incubation, a significant increase from 1 Hz to 5 Hz ($P < 0.002$) and from 5 Hz to 10 Hz ($P < 0.002$) was observed. A change from 5 Hz to 10 Hz, saw the loss modulus

increasing significantly (P < 0.004) in the MGO group before incubation. No change was detected in the MGO group after treatment over the selected frequencies. Comparing the same groups after treatment, the glycated group showed a significant increase (P < 0.05) in the loss modulus at 1.0 Hz. Figure 33 shows the boxplots of the mean values of the loss modulus of both control and MGO groups, before and after incubation over the four selected frequencies. The loss modulus showed a similar behavior to the loss tangent with frequency for both groups before and after incubation.

Table 3: the mean values ± the standard deviation of the loss modulus in MPa, for both control and test group before and after incubation. A significant increase (P< 0.05) in the loss modulus in the MGO groups can be observed after incubation at 1.0 Hz.

Loss modulus (Mean value) [MPa]				
Frequency [Hz]	0.5	1.0	5.0	10
Control group pre-incubation N = 9	0.144 ± 0.14	0.107 ± 0.073	0.143 ± 0.078	0.141 ± 0.068
Control group post-incubation N = 9	0.143 ± 0.16	0.121 ± 0.11	0.153 ± 0.11	0.190 ± 0.12
MGO group pre-incubation N = 9	0.096 ± 0.090	0.091 ± 0.043	0.095 ± 0.024	0.123 ± 0.043
MGO group post-incubation N = 9	0.144 ± 0.14	0.133 ± 0.067	0.155 ± 0.12	0.164 ± 0.12
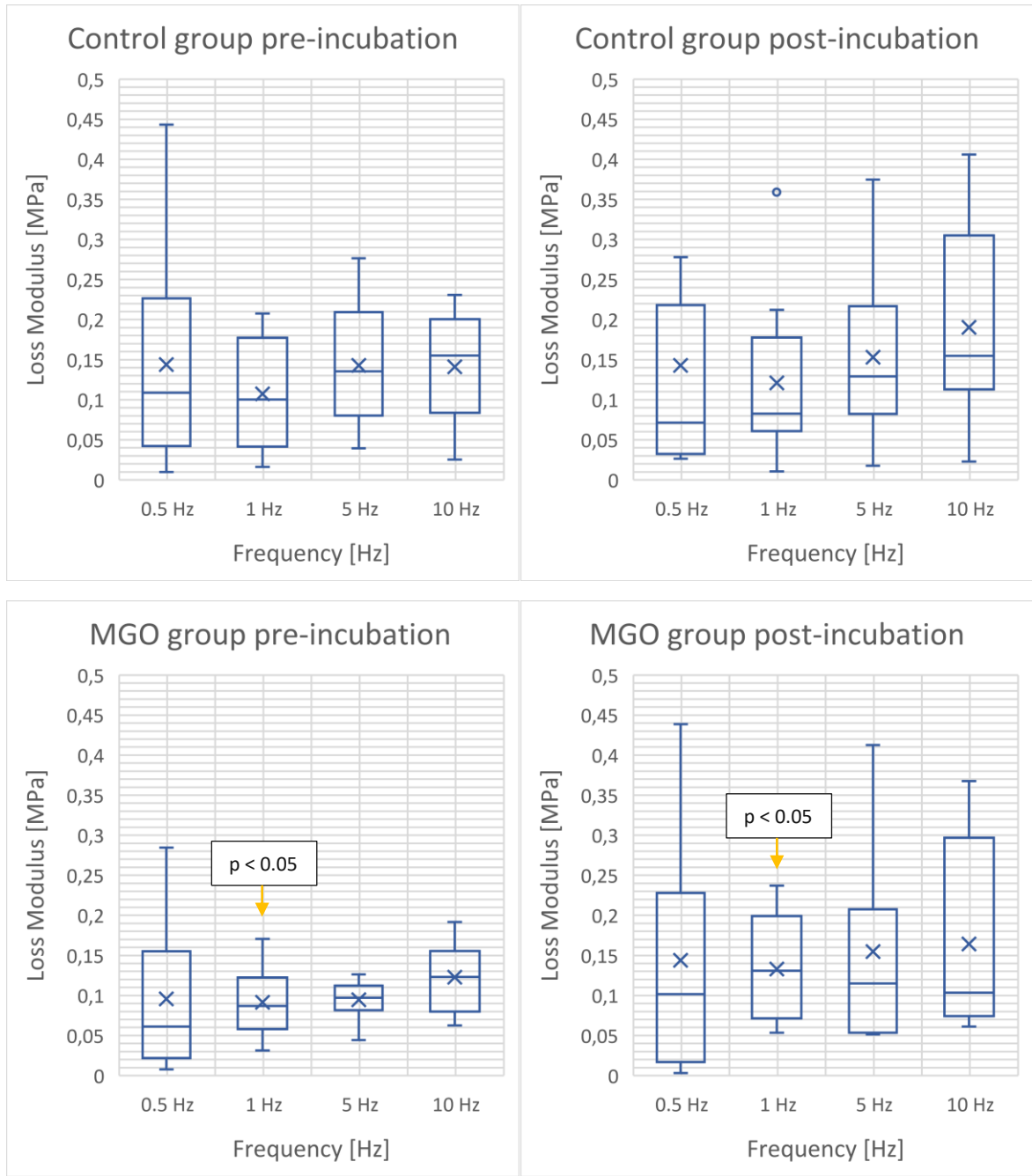
Figure 33: Boxplots of the mean values of the loss modulus for both groups before and after incubation.

The dynamic modulus showed only a change at 10 Hz in the control group comparing the before and after incubation groups ($P < 0.05$). Table 4 shows the mean values $\pm$ the standard deviation of the dynamic modulus of the 9 fibrils for both groups over the selected four frequencies.

Figure 34 shows the boxplots of the mean values of the dynamic modulus of the 9 fibrils for both groups over the selected four frequencies. The values of the dynamic modulus are almost constant over frequency for both groups before and after incubation.

Table 4:   the mean values $\pm$ the standard deviation of the dynamic modulus of the 9 fibrils for both groups over the selected four frequencies.

Dynamic modulus (Mean value) [MPa]				
Frequency [Hz]	0.5	1.0	5.0	10
Control group pre-incubation N = 9	1.45 ± 0.80	1.35 ± 0.63	1.42 ± 0.67	1.39 ± 0.59
Control group post-incubation N = 9	1.50 ± 0.67	1.52 ± 0.66	1.65 ± 0.74	1.67 ± 0.68
MGO group pre-incubation N = 9	2.19 ± 0.73	2.02 ± 0.58	1.88 ± 0.51	1.90 ± 0.58
MGO group post-incubation N = 9	2.29 ± 0.96	2.02 ± 0.76	2.11 ± 0.66	2.08 ± 0.84
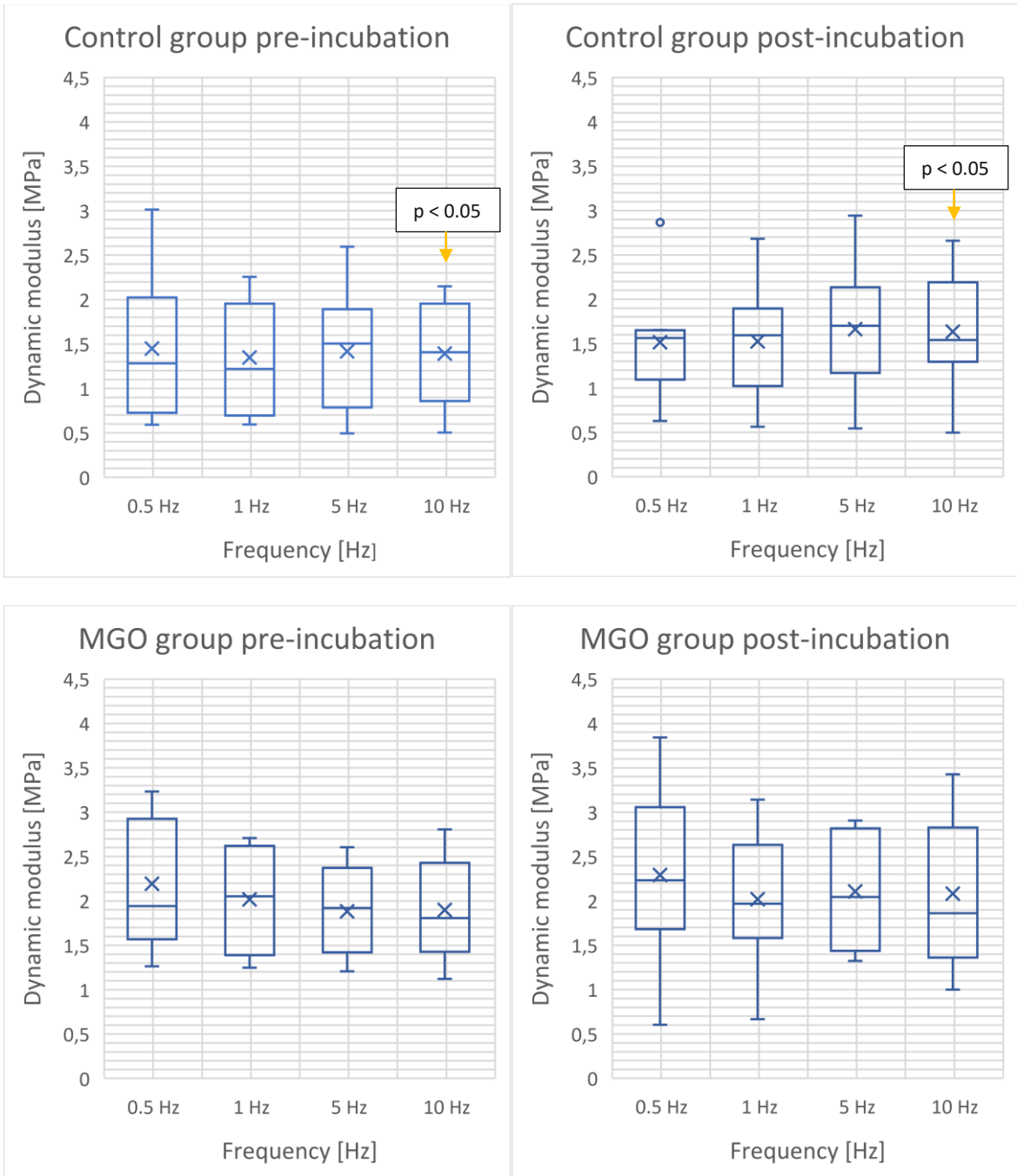
Figure 34: Boxplots of the mean values of the dynamic modulus in MPa, of 9 fibrils for both control and test group before and after incubation. The mean values are almost constant over frequency.

In addition to the results from the dynamic nanoindentation, the indentation modulus E of the 9 fibrils in each group before and after incubation were calculated from the simple indentation measurements. The results showed that the mean value of indentation modulus of the control group went from (1.5 ± 1.1) MPa to (1.47 ± 0.55) MPa after incubation ($P < 0.5$). Whereas for the MGO group from (1.91 ± 0.85) MPa to (2.11 ± 0.66) MPa after incubation ($P < 0.2$). There was no significant change in the indentation modulus for both groups after incubation. Figure 35 shows the boxplots of the mean values of the indentation modulus of both control and MGO group, before and after incubation.
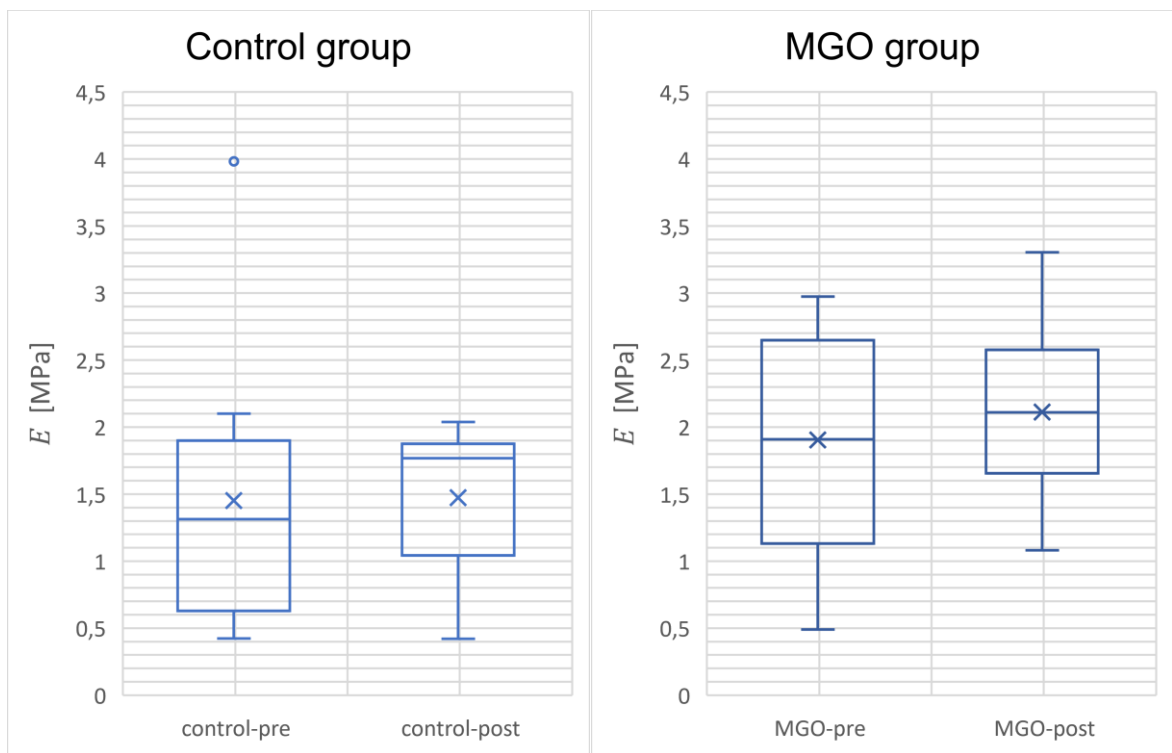
Figure 35: Boxplots of the mean values of the indentation modulus of both groups before and after incubation from 9 fibrils in each group.

The swelling behavior was also investigated for the individual collagen fibrils in each group before and after incubation (N = 9 for each group) as it is an important phenomenon in biological tissues. Images of the dry fibrils were taken in air using the contact mode to get the dry diameters of each fibril. Whereas from the simple indentation measurements in PBS, the wet diameter of each fibril could be obtained. The results showed that the mean values ± the standard deviation of the dry diameters of the control group went from (117 ± 21) nm to

(113 ± 24) nm after incubation, while for the MGO group the dry diameters went from (116 ± 29) to (118 ± 28) after incubation. For the wet diameters the mean values ± the standard deviation of the control group went from (174 ±37) to (181 ±31), while for the MGO group the wet diameters went from (170 ±64) to (166 ±32) (see Figures 36 and 37)

The mean value of the swelling ratio (D_{wet}/D_{dry}) of the control group went after incubation from (1.51 ± 0.34) to (1.64 ± 0.36), while for the MGO group the mean value went from (1.45 ± 0.27) to (1.44 ±0.22) (see Figure 38).
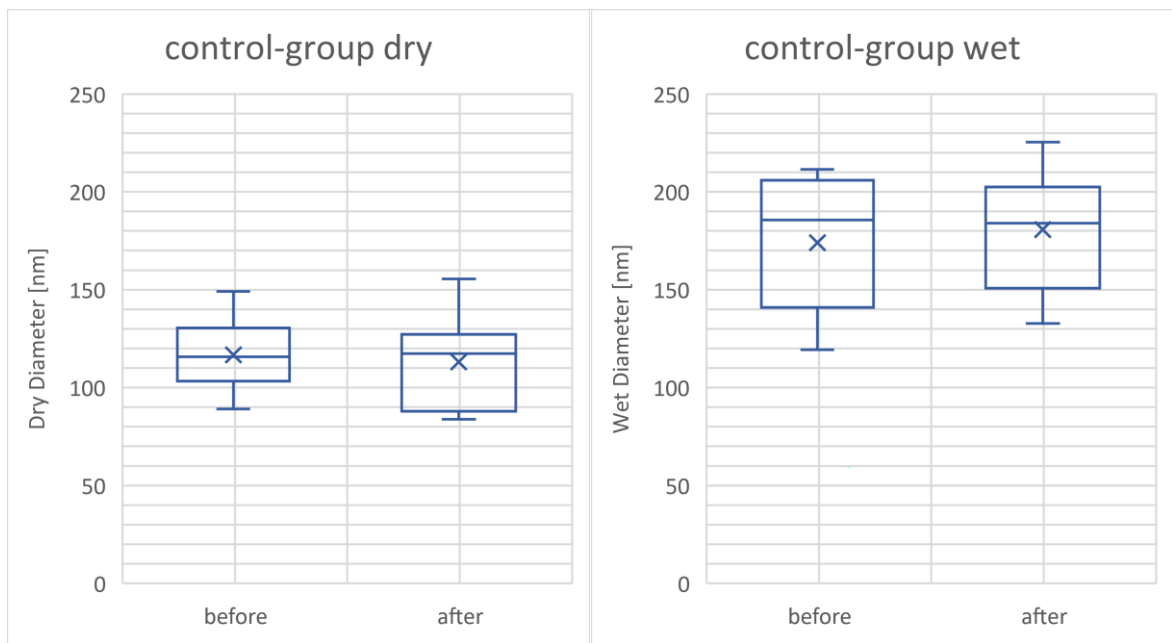
Figure 36: the values of the dry diameters of the control group before and after glycation are shown to the left, while the values of the wet dimeters of the control group before and after incubation are shown to the right.
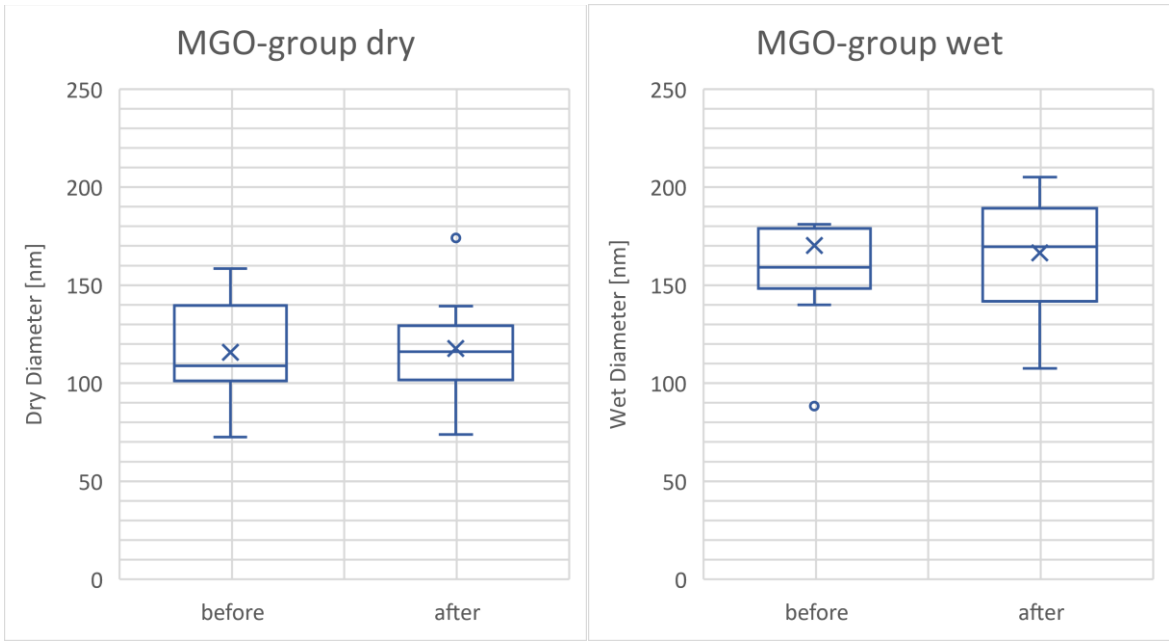
Figure 37: The values of the dry diameters of the MGO group before and after glycation are shown to the left, while the values of the wet dimeters of the MGO group before and after incubation are shown to the right
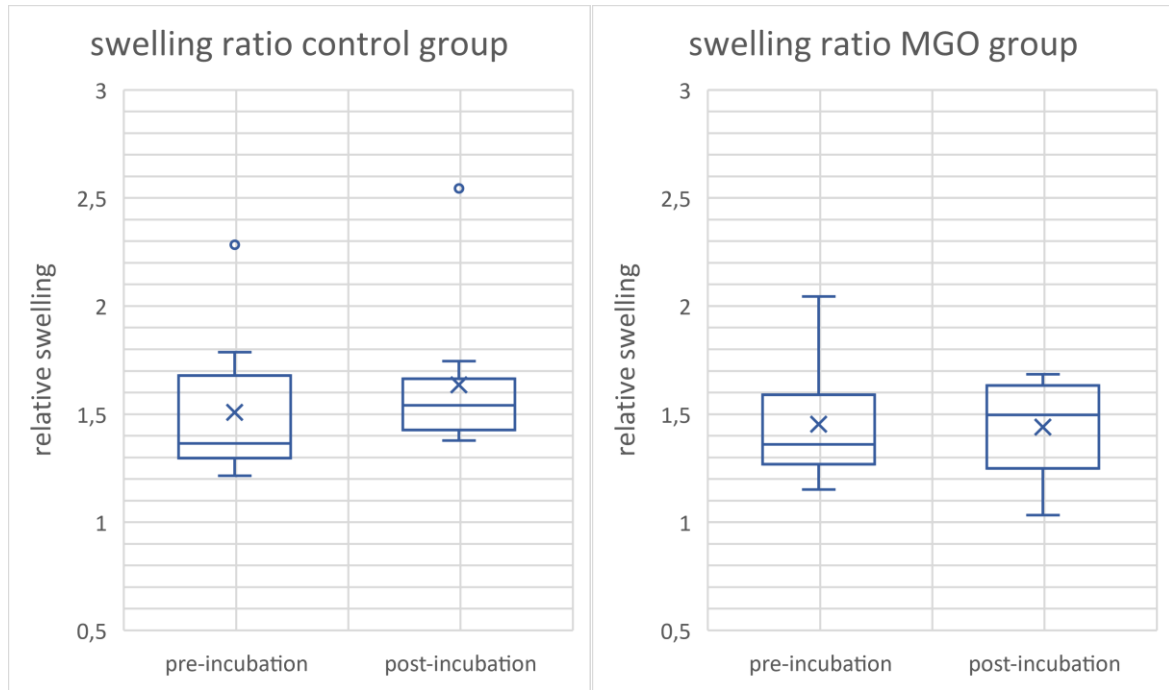
Figure 38: The swelling ratio of the fibrils before and after incubation can be seen with control group to the left and the MGO group the right.

5.2 Dynamic tensile testing results

After measuring the 10 fibrils on each group with the AFM before and after incubation, the two slides were measured using the NanoTens device. The fibrils of the MGO group showed that they may be tougher than the fibrils of the control group. As 7 treated fibrils from 13 could be measured while the rest of the fibrils either ruptured before measuring or it was hard to measure them (as some were too short, or the glue points were too big, which hindered the micro gripper). For the control group most of the fibrils ruptured before measuring and a supplementary control slide was needed and prepared from the same mouse tail tendon fascicle for the sake of data completeness. The initial lengths of the fibrils were measured using the light microscope, while their hydrated diameters were obtained from the AFM nanoindentation measurements. A dynamic mechanical analysis (DMA) was performed on each individual fibril from each group at 0.05, 0.1, 0.5 and 1.0 Hz at force set point of 1 µN and 2 µN. Then tensile test in open loop mode with strain rate 5%/s followed until fibril rupture. Through DMA measurements, the following parameters could be calculated: the loss tangent, storage and loss modulus, and dynamic modulus. From the results of the tensile tests, forces, stresses, strains, ultimate strengths and tensile moduli could be calculated.

The mean values ± the standard deviation of the loss tangent of the control and MGO groups at both 1 µN and 2 µN force set points can be seen in table 5. Looking at the behavior of the loss tangent of each group over frequency, one can see the following: a significant increase in the loss tangent for the control group at set point 1 µN from 0.05 Hz to 0.1 Hz ($P < 0.05$) was observed, while from 0.1 Hz to 0.5 Hz a significant decrease ($P < 0.0001$) was detected. The loss tangent of the control group at set point 2 µN showed a significant decrease ($P < 0.0003$) going with frequency from 0.1 Hz to 0.5 Hz. For the MGO group both measurement at 1 µN ($P < 0.01$) and 2 µN ($P < 0.003$) showed a significant decrease in the loss tangent with increasing the frequency from 0.1 Hz to 0.5 Hz. The loss tangent values of the MGO groups at 1 µN set point showed to have less values than the control group, at 0.1 Hz ($P < 0.04$), 0.5 Hz ($P < 0.03$) and 1 Hz ($P < 0.02$), while at the 2 µN this was also clear at 1.0 Hz ($P < 0.05$).

Table 5:   the mean values ± the standard deviation of the loss tangent at the selected frequencies of both control and MGO groups at a force setpoint of 1 µN and 2 µN.

Loss Tangent (Mean value)				
Frequency [Hz]	0.05	0.1	0.5	1.0
Control group Set point= 1 µN N = 8	0.20 ± 0.07	0.23 ± 0.06	0.085 ± 0.038	0.081 ± 0.036
Control group Set point= 2 µN N = 7	0.16 ± 0.09	0.20 ± 0.04	0.076 ± 0.043	0.078 ± 0.035
MGO group Set point= 1 µN N = 6	0.15 ± 0.08	0.16 ± 0.07	0.054 ± 0.015	0.047 ± 0.006
MGO group Set point= 2 µN N = 5	0.16 ± 0.06	0.17 ± 0.04	0.051 ± 0.02	0.052 ± 0.04

Figure 39 shows the boxplots of the mean values of the loss tangent of both control and MGO groups at force set point of 1 µN with significant decrease of the loss tangent in both groups with increasing the frequency from 0.1 Hz to 0.5 Hz. While Figure 40 displays the boxplots of the mean values of the loss tangent of both groups at force set point of 2 µN with significant decrease in the loss tangent with increasing the frequency from 0.1 Hz to 0.5 Hz.
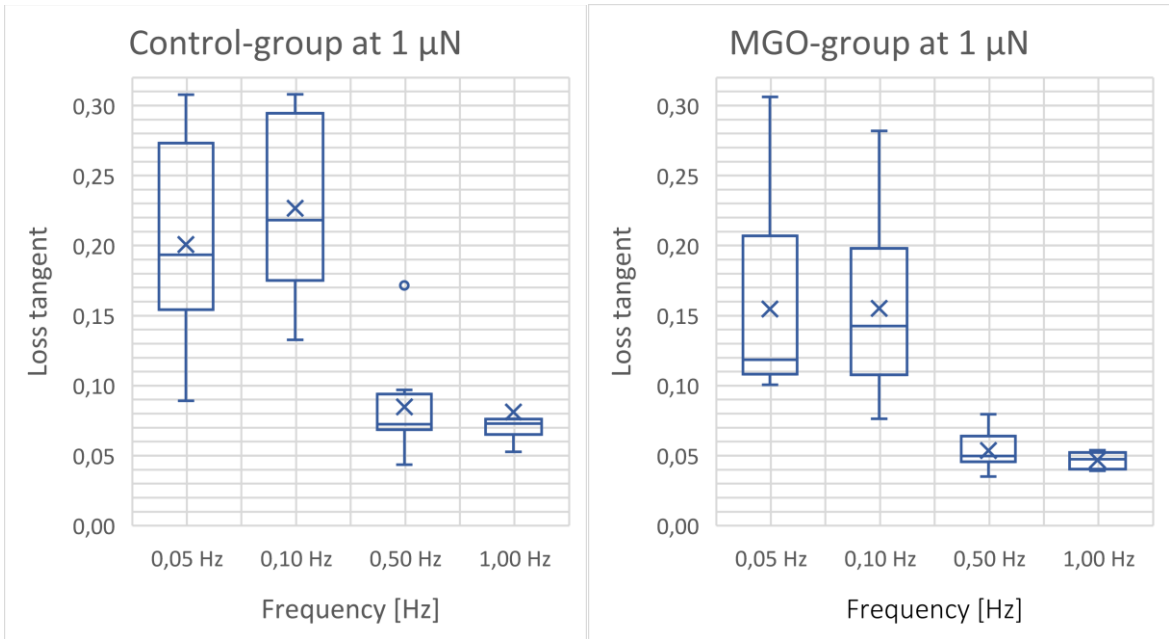
Figure 39: The values of the loss tangent at the selected frequencies at 1 µN force set point, the control group to the left and the MGO group to the right.
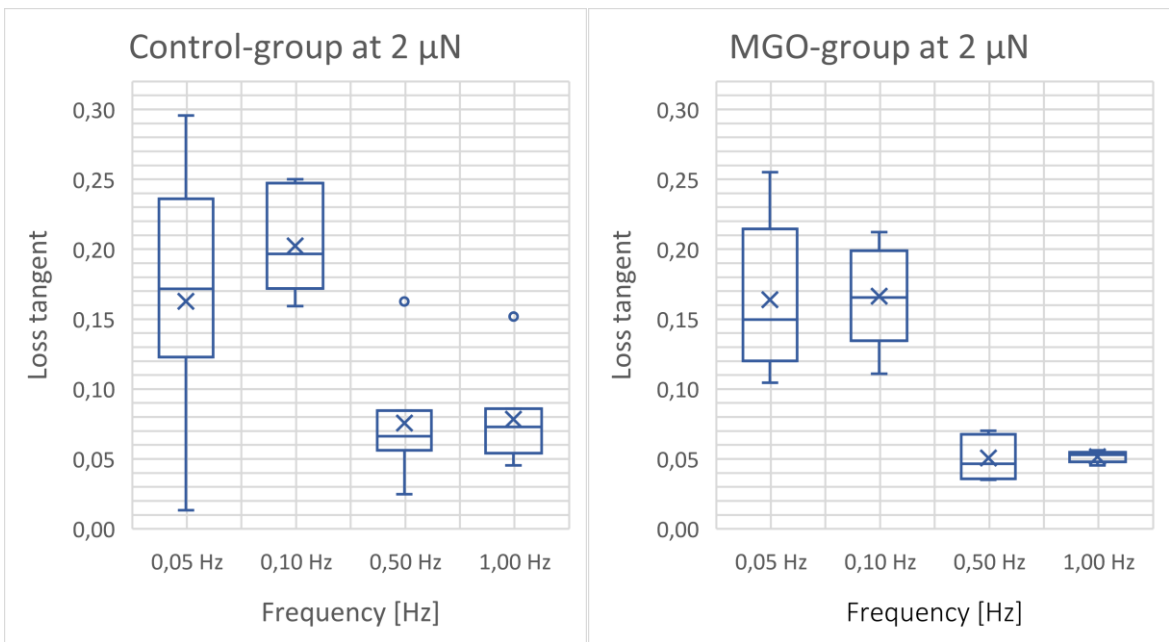
Figure 40: The values of the loss tangent at the selected frequencies at 2 µN force set point, the control group to the left and the MGO group to the right.

Table 6 shows the mean values ± the standard deviation of the dynamic modulus of the control and MGO groups at both 1 µN and 2 µN force set points. No significant change can be detected over frequency in the dynamic modulus in each group as well as when comparing the control group with the MGO group. Pooling all the data of the control group, and all the

data of the MGO group over the four frequencies and comparing both groups statistically at 1 μN (P < 0.1) and 2 μN (P < 0.2) set points, showed nonsignificant differences between both groups. The boxplots of the mean values of the dynamic modulus of both control and MGO groups at force set point of 1 μN can be seen in Figure 41 and for the control and MGO groups at force set point of 2 μN in Figure 42.

Table 6:   the mean values ± the standard deviation of the loss tangent at the selected frequencies of both control and MGO groups at a force setpoint of 1 μN and 2 μN.

Dynamic modulus (Mean value) [MPa]				
Frequency [Hz]	0.05	0.1	0.5	1.0
Control group Set point= 1 μN N = 7	2.95 ± 1.3	2.92 ± 1.2	3.0 ± 1.2	3.12 ± 1.3
Control group Set point= 2 μN N = 6	3.85 ± 1.9	3.72 ± 1.8	3.80 ± 1.7	3.90 ± 1.7
MGO group Set point= 1 μN N = 5	3.62 ± 1.7	3.41 ± 1.6	3.46 ± 1.6	3.49 ± 1.6
MGO group Set point= 2 μN N = 5	4.29 ± 1.8	4.16 ± 1.5	4.12 ± 1.7	4.23 ± 1.7
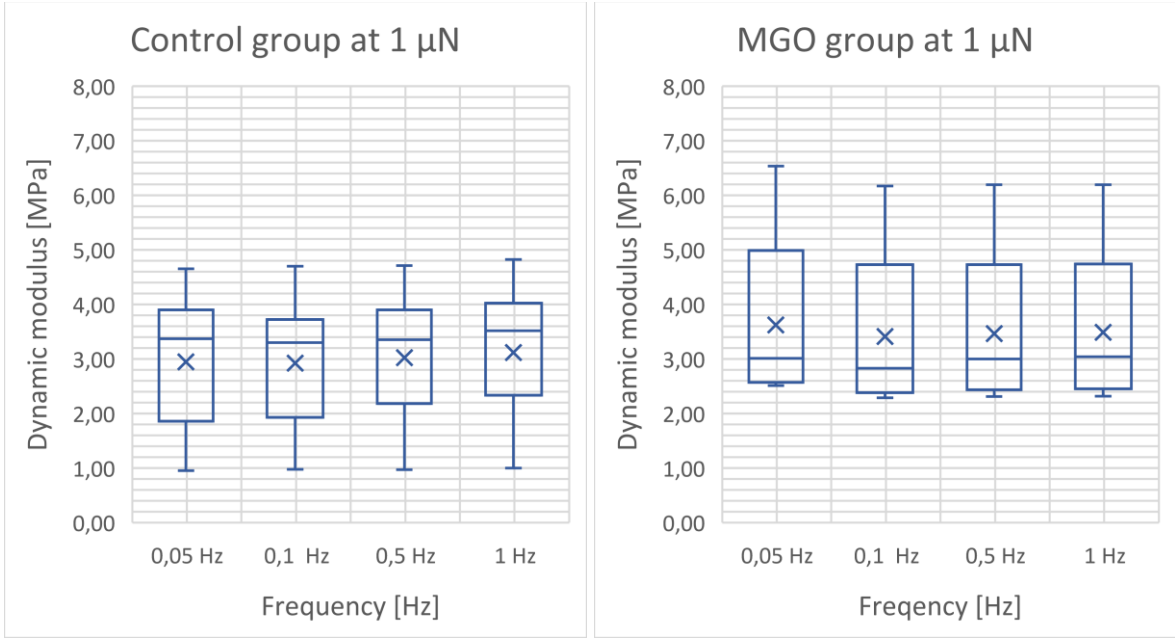
Figure 41: The values of the dynamic modulus at the selected frequencies at 1 µN force set point, the control group to the left and the MGO group to the right.
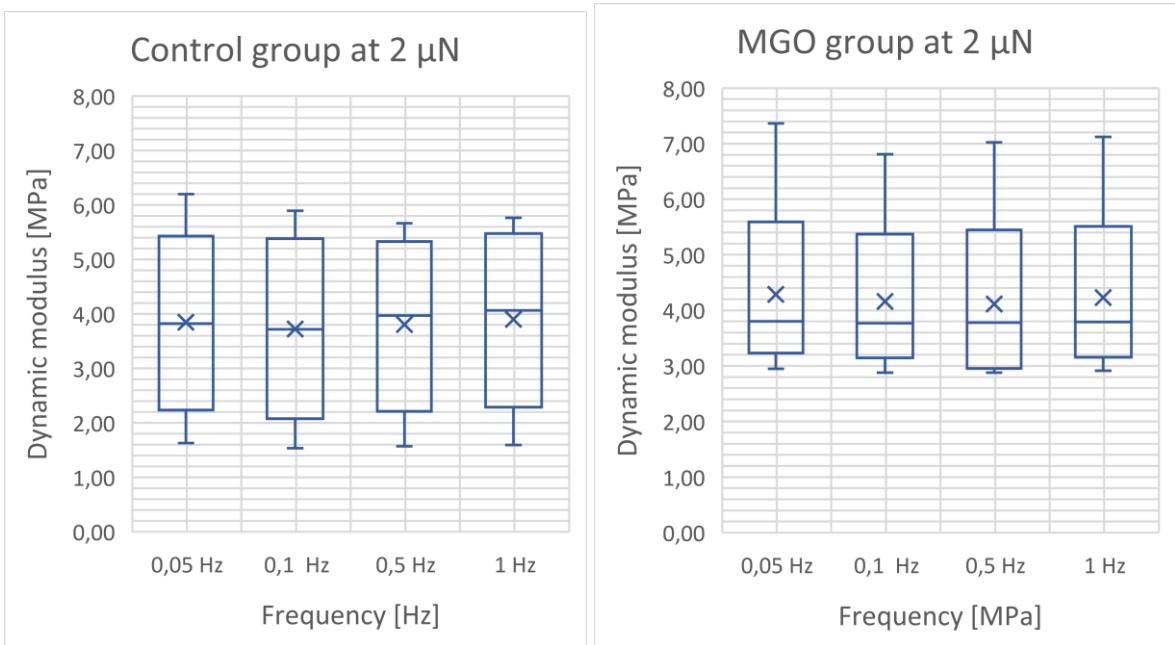
Figure 42: The values of the dynamic modulus at the selected frequencies at 2 µN force set point, the control group to the left and the MGO group to the right.

After applying DMA on each fibril from both groups, a tensile test in open loop mode with strain rate of 5%/s was performed on each individual fibril until rupture. The stress-strain curves of fibrils from both control and MGO group (N= 4 in each group) are shown in Figure 43. The measured values of ultimate force (F), ultimate stress (σ) and ultimate strain (ε) are shown with the measured values of the hydrated fibrils diameters and their initial measured lengths in tables 7 and 8 for the control (N=4) and MGO (N=4) groups respectively. The collagen fibrils of the control group reached a peak force of 14 ± 5 µN, while the fibrils of the MGO group reached a peak force of 20 ± 14 µN. The ultimate tensile strengths of the same fibrils were calculated by normalizing the forces with the areas of the hydrated collagen fibrils (assuming a circular cross section, with the hydrated diameters measured via AFM nanoindentation). Both groups showed the same value of ultimate tensile strength at different values of strain: (0.89 ± 0.46) GPa at (32 ± 11) % strain for the control group, and (0.89 ± 0.71) GPa at (25 ± 9) % strain for the MGO group.
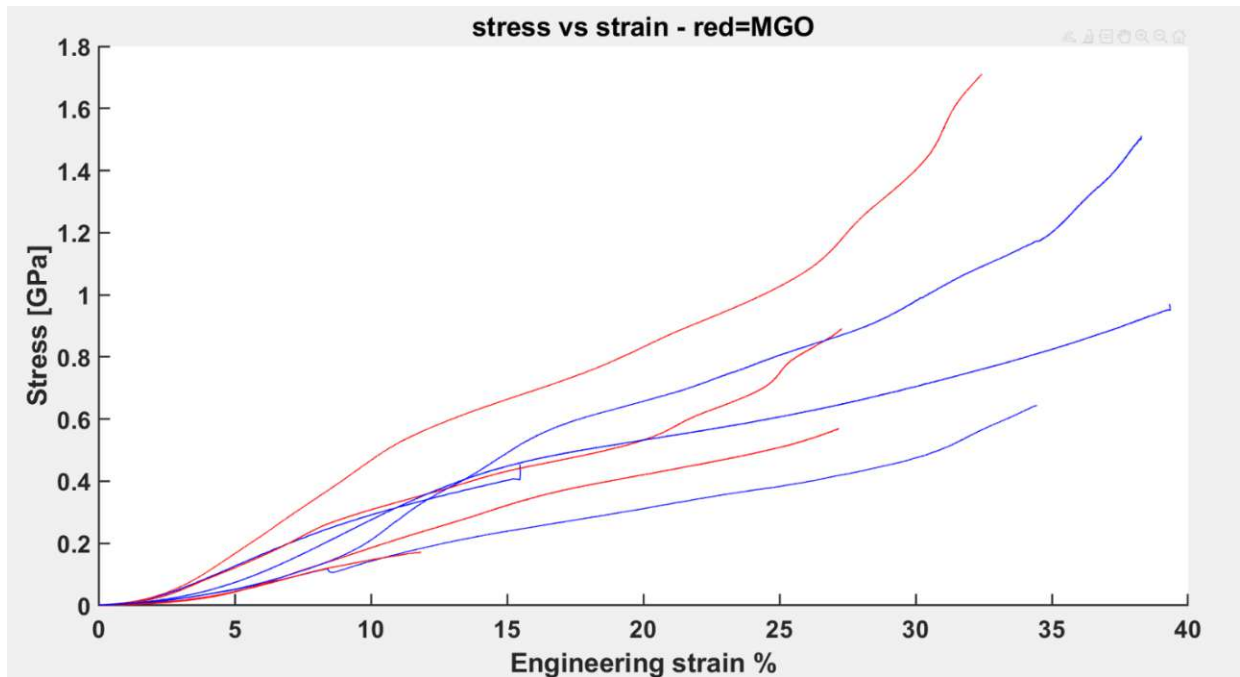
Figure 43: Stress-strain curves of fibrils from control (N = 4, blue) and MGO (N = 4, red) groups

Table 7: The measured values of the ultimate: force (F), stress (σ) and strain (ε), the hydrated fibrils diameter with their initial length of the control group (N=4).

Control group	F_{ult} [µN]	σ_{ult} [GPa]	ε_{ult}[%]	Diameter [nm]	Length [µm]
S1_F2	8.18	0.45	15.50	152.14	173.10
S1_F7	17.60	0.64	34.28	187.19	124.0
S3_F2	17.96	1.51	38.28	123.10	114.74
S4_F4	10.31	0.97	39.31	116.36	70.35
Mean ± SD	**14** ± 5.0	**0.89** ± 0.46	**32** ± 11	**145** ± 32	**121** ± 42

Table 8: The measured values of the ultimate: force (F), stress (σ) and strain (ε), the hydrated fibrils diameter with their initial length of the MGO group (N=4).

MGO group	F_{ult} [µN]	σ_{ult} [GPa]	ε_{ult}[%]	Diameter [nm]	Length [µm]
S2_F4	12.69	0.57	27.16	168.39	72.08
S2_F5	32.35	0.98	27.25	205.05	75.06
S2_F8	29.92	1.84	32.43	143.93	116.88
S2_F10	3.89	0.17	11.84	170.65	80.89
Mean ± SD	**20** ± 14	**0.89** ± 0.71	**25** ± 9.0	**172** ± 25	**86** ±21

5.3   AFM nanoindentation vs. NanoTens dynamic tensile tests

Looking at the same fibrils examined with both instruments of both control and MGO groups was important to compare the paired data. In table 9 the loss tangent of the control group from AFM and NanoTens measurements at the frequencies in common (0.5 Hz and 1.0 Hz), are highlighted and showed comparable values in both experiments. Table 10 gives an overview of the loss tangent of the MGO group from both AFM and NanoTens measurements. The values at the frequencies in common (0.5 Hz and 1.0 Hz) are highlighted.

Table 9:   the mean values ± the standard deviation of the loss tangent of the control group from AFM (before and after incubation) at the selected frequencies, and from the DMA (at 1 µN and 2 µN) at the selected frequencies with the common frequencies between both groups

Loss Tangent (Mean value)							
	Frequency [Hz]	0.05	0.1	0.5	1.0	5.0	10
AFM	Control group pre-incubation N = 9			0.104 ± 0.088	0.071 ± 0.025	0.098 ± 0.014	0.098 ± 0.022
	Control group post-incubation N = 9			0.086 ± 0.056	0.074 ± 0.039	0.086 ± 0.029	0.109 ± 0.040
NanoTens	Control group Set point= 1 µN N = 8	0.20 ± 0.07	0.23 ± 0.06	0.085 ± 0.038	0.081 ± 0.036		
	Control group Set point= 2 µN N = 7	0.16 ± 0.09	0.20 ± 0.04	0.076 ± 0.043	0.078 ± 0.035		

Table 10: the mean values ± the standard deviation of the loss tangent of the MGO group from AFM (before and after incubation) at the selected frequencies, and from the NanoTens DMA (at 1 µN and 2 µN) at the selected frequencies with the commen frequencies between both groups

Loss Tangent (Mean value)							
	Frequency [Hz]	0.05	0.1	0.5	1.0	5.0	10
AFM	MGO group pre-incubation N = 9			0.055 ± 0.036	0.048 ± 0.015	0.056 ± 0.014	0.073 ± 0.014
	MGO group post-incubation N = 9			0.086 ± 0.065	0.071 ± 0.032	0.072 ± 0.043	0.075 ± 0.037
NanoTens	MGO group Set point= 1 µN N = 6	0.15 ± 0.08	0.16 ± 0.07	0.054 ± 0.015	0.047 ± 0.01		
	MGO group Set point= 2 µN N = 5	0.16 ± 0.06	0.17 ± 0.04	0.051 ± 0.02	0.052 ± 0.04		

Comparing the moduli (tensile, indentation) of the paired data of individual fibrils from both control and MGO groups as shown in table 11, and using the Pearson correlation coefficient, a non significat large positive relation between both moduli ($r(3) = 0.795$, ($P < 0.1$)) was detected as shown in Figure 44.

Table 11: tensile modulus (first local maximum) from NanoTens and indentation modulus from AFM of the same fibrils from the quasi-static tensile test

	Tensile modulus [GPa]	Indentation modulus [MPa]
Control group		
S1_F2	3.83	1.84
S1_F7	2.75	1.37
MGO group		
S2_F4	3.03	2.11
S2_F5	3.81	2.28
S2_F10	2.41	1.08
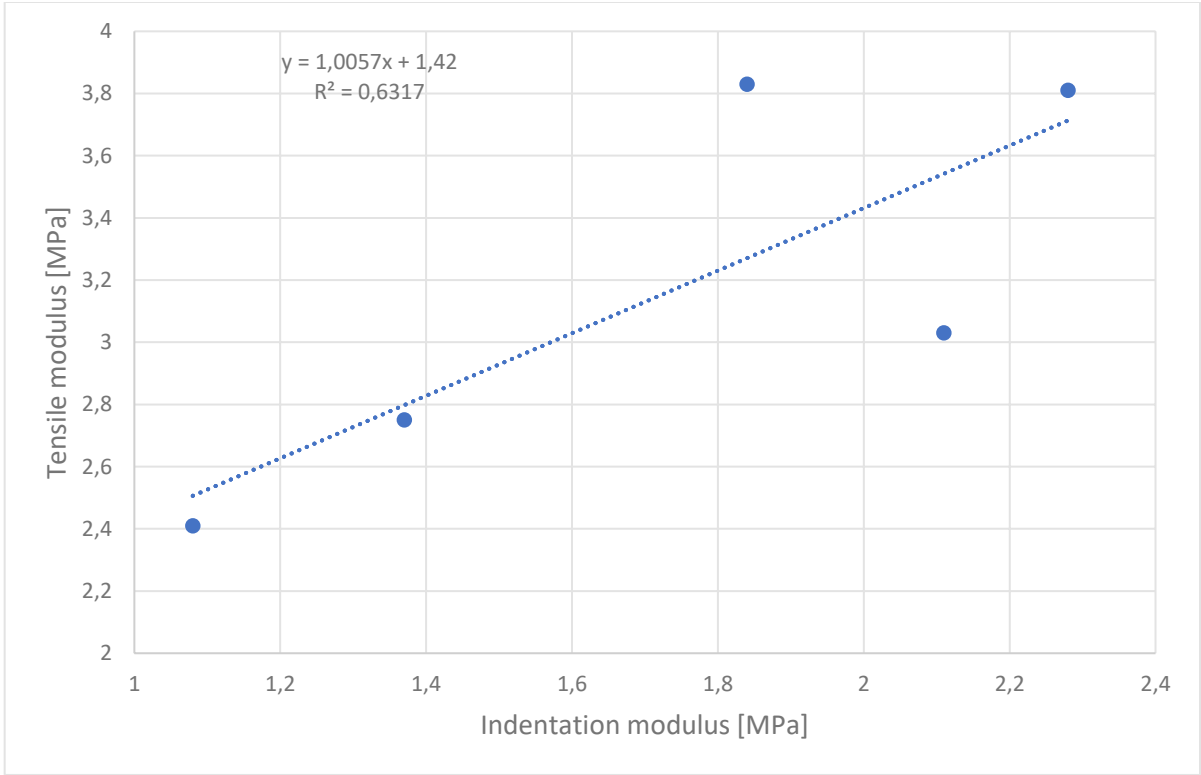
Figure 44: tensile modulus from NanoTens vs. indentation modulus from AFM of the same fibrils from the quasi-static tensile tests showing a non significat large positive relation between both moduli (r(3) = 0.795, (P < 0.1))

6 Discussion

This study was designed to examine the effects of glycation on the viscoelastic behavior in individual collagen fibrils. This was achieved using two different methods: AFM and tensile testing. Two groups of fibrils were prepared from the same fascicle, which was extracted from a WT mouse tail tendon so that the very same fibrils can be investigated. A test group was prepared using MGO as a cross-linking agent to mimic the effects of AGEs in elders and diabetic patients. Whereas the control group was used as a reference and to reduce any changes unrelated to glycation through the whole experiment.

6.1   AFM dynamic nanoindentation

AFM active microrheology method showed that it is a powerful method with a large available range of forces and frequencies that can be applied through different experiments. However, this method has a drawback, which is the low acquisition speed, which can last for several hours. In this experiment a dynamic oscillatory indentation testing at a range of physiologically relevant frequencies were applied on the single fibrils. The lower frequencies (< 0.5 Hz) could not be measured due to the noise in both indentation and force signals, which hindered the data acquisition. The results of this method showed that, both the loss modulus and the loss tangent of the control group before and after incubation as well as the MGO group before incubation are frequency dependent. The control group after incubation showed an increase with frequency from 1.0 Hz to 10 Hz, while before incubation they only increased in the range from 1.0 Hz to 5 Hz. For the MGO group the increase was with increasing the frequency from 5 Hz to 10 Hz just before incubation. This dependency of the loss tangent and loss modulus on frequency is in agreement with the findings of previous studies [5, 9]. In the study of Yuri M. Efremov, a dynamic oscillatory indentation with frequencies in the range from 0.001-100 kHz were conducted on biological cells and the results showed the dependency on frequency. Both the loss and storage modulus, and the loss tangent increased with increasing frequency. Whereas in the study of Colin A. Grant a low frequency range (0.1 Hz - 2 Hz) dynamic mechanical analysis on individual collagen fibrils has been carried out using atomic force microscopy on both gap and overlap regions

on single fibrils. The calculated phase shift showed dependency on frequency, that is the phase shift increased with frequency.

While this frequency dependency in the current study could be measured in the control group before and after incubation, and in the MGO group before incubation, the latter showed no changes with changing the frequency after incubation. This may indicate an effect due to glycation. Comparing the same group before and after incubation, the MGO group showed a change in the loss tangent and loss modulus values at 1.0 Hz after glycation.

Looking at a microrheology simulation model with a varying viscosity as shown in Figure 45, the different phase shift curves with increasing the frequency can be seen in figure 46. The simulation was done in MATLABs SIMULINK using SIMSCAPE functionalities.

In this model a standard linear solid (SLS) model (a spring in parallel with a Maxwell element) was used, and a modulation signal at multiple specific frequencies was applied through an AFM tip, which was modelled as an idealized spring.

Comparing the resulted phase shift curves of the experiment simulation of this model with the loss tangent values of the different fibril groups of the current study revealed the following:

The loss tangent values of all the groups except for the MGO after incubation showed to be in the rising phase of the curve with increasing frequency (for example the yellow curve in Figure 46). While the values of the loss tangent of the MGO group after incubation showed to be constant with frequency, which means that this may be the peak of the curve at the same frequency range (for example the red curve in Figure 46). This shows that there may be a shift back of the phase shift curve in the frequency domain in case of MGO group after incubation, which may indicate an increase in the viscosity of the treated fibrils due to glycation. Although this model was using arbitrary values for the mechanical components (springs, dashpot, etc.) and the comparison is only qualitative, the result of this simulation is in agreement with the trends the loss tangent showed in the real data of this work.
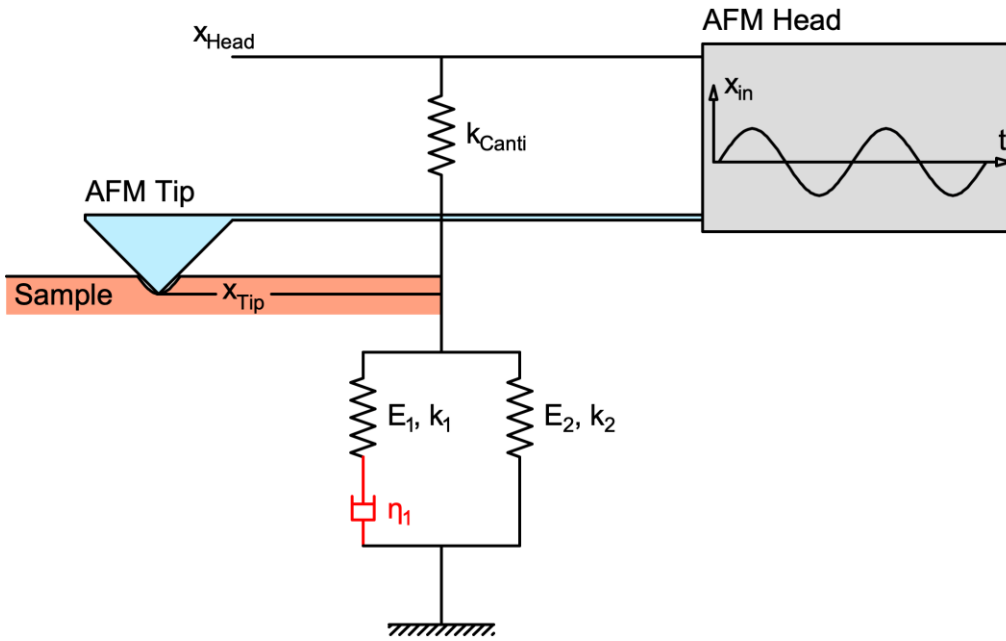
Figure 45: microrheology simulation experiment, showing an SLS model with an applied modulation signal through AFM tip (courtesy of Manuel Rufin and Simon Jaritz)
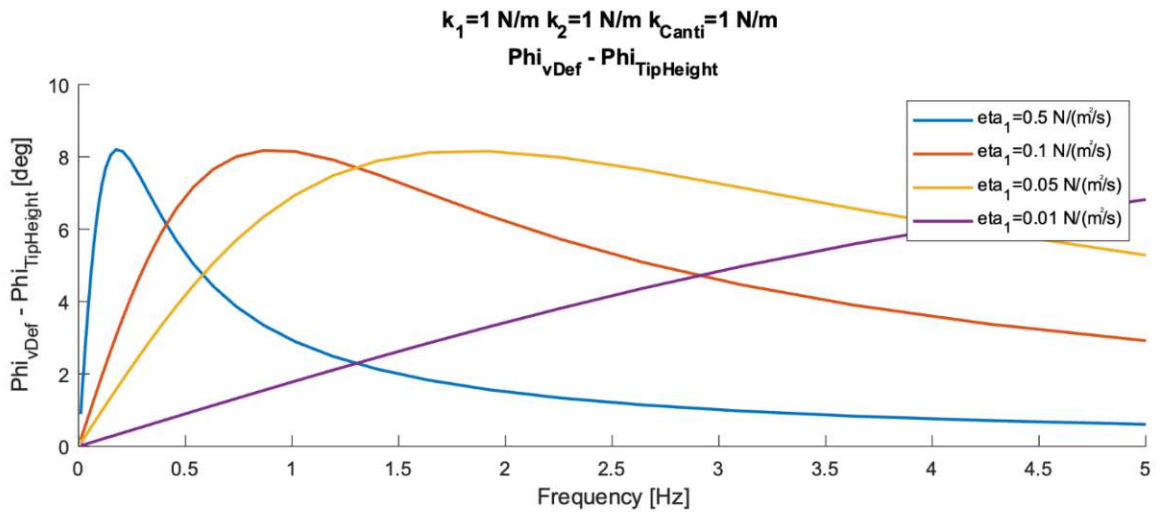
Figure 46: curves of the phase shift over frequency for different viscosities (courtesy of Manuel Rufin and Simon Jaritz)

For the storage modulus, the control group after incubation showed an increase with increasing the frequency from 1.0 Hz to 5 Hz while for the MGO group before incubation it decreased. There was an increase in the storage as well as the dynamic modulus in the control group after incubation at 10 Hz.

Also, the AFM static nanoindentation results showed that there was no change in the indentation modulus after incubation for both groups. The result of the MGO group is inconsistent with the study of Rufin, M., which was done on collagen fibrils that were extracted from WT mouse tail tendon and showed a significant increase in case of MGO glycated fibrils compared the control group using a similar protocol to the one used in the current study.[12] However, it agrees with the study of Gion Fessel, where collagen fibrils from rat- tail tendon with introduced AGEs showed that there is no change in fibril modulus, surprisingly and contradictory to the widespread assumption that tissue stiffening in aging and diabetic patient is directly related to AGE increased fibril stiffness.[19]

The swelling behavior in the present study for both control and MGO did not show any change after incubation in the relevant solutions. Also, there was no significant change in the dry and wet diameters of both groups after incubation. This may indicate that the incubation in the MGO solution was ineffective.

6.2   Dynamic tensile tests

Dynamic mechanical analysis (DMA) using the NanoTens instrument showed that there seem to be effects of MGO induced glycation in individual collagen fibrils. The results suggest that the MGO group has lower dissipation and is less viscous at the examined frequencies (0.1-1.0 Hz). The ultimate strength of the MGO group showed the same value as of the control group but at lower strain compared to the control group. An ultimate strength of (0.89 ±0.46) GPa at (32 ± 11) % strain for the control group, while (0.89 ± 0.71) GPa at (25 ± 9) % strain for the MGO group. This can indicate an effect of glycation on the fibrils and agrees with the study of Rene B. Svensson, which examined the effects of maturation and glycation on tensile mechanics of collagen fibrils from mouse tail and Achilles tendons. The study showed that MGO treatment increased strength and stiffness of the glycated fibrils leading to stronger and tougher fibrils.[22]

6.3   AFM dynamic nanoindentation vs. Dynamic tensile test

Through both measurements different mechanical parameters could be calculated and further analyzed. Comparing both experiments, the results showed some differences. This can be explained by the different measurement protocols of each experiment: While the DMA

tensile testing using the NanoTens devise examined the fibrils in their loading direction (long axis), the AFM measurements were performed radially. Moreover, the range of frequencies of both techniques only overlapped partially. An important range of frequencies (< 0.5 Hz) was hard to be investigated using the AFM nanoindentation as the measurements at this range are very noisy. On the contrary, while the lower frequencies (< 0.5 Hz) are more feasible with the NanoTens than with AFM, higher frequencies can currently not be examined using this method. Furthermore, the application modes of the modulation signals differ. In AFM they were applied starting from the highest frequency, while using the NanoTens the application started with the lower ones. However, each measurement has its advantages and disadvantages. For AFM the measurements on the fibrils are reproducible and can be conducted several times with different configurations on the very same spot on the fibril. One of the shortcomings of this method is the low acquisition speed resulting in long measurement times that can last for hours. On the other hand, the dynamic tensile testing measurement using NanoTens device is easy to conduct with fast sample loading and unloading. It can be performed in a very short time (5 minutes per fibril) compared to AFM. The measurements are also reproducible unless the fibril ruptures, which needs some expertise to be avoided. The shortcoming of this method is the extra sample preparation, which must be conducted with certain conditions to make the loading of the fibril on the microgripper easy and possible.

A challenge in this study was to decide the workflow. While measurements using the AFM are sophisticated and time consuming, the NanoTens device often ruptures the fibrils. Here the question arose which measurement to complete first, since starting with the AFM risks damage to the fibril in the NanoTens device afterwards thus making the AFM measurements useless in our comparison. On the other hand, performing the tensile test first makes the AFM measurement much harder since it requires a long search for the intact part in the fibril to perform AFM measurement due to the fibrils being damaged in the preceding step. In the current study, measurements with AFM were conducted first, then the Tensile test using the NanoTens instrument followed. After measuring with AFM, most of the fibrils of the control group ruptured while measuring with the NanoTens, which demanded a supplementary control slide.

7 Conclusion

In this work, atomic force microscopy dynamic nanoindentation as well as tensile dynamic testing using the NanoTens instrument have been used to examine the implications of glycation on the nanomechanical, viscoelastic properties in individual collagen fibrils from a WT mouse tail tendon under physiological conditions (fully hydrated in PBS).

Two groups of fibrils were prepared, a control group and a test group simulating the presence of AGEs in the individual collagen fibrils. For the AFM dynamic nanoindentation measurements, a force ramp protocol was designed to examine the viscoelastic behavior of individual fibrils using physiologically relevant frequencies. The lower range of frequencies (below 0.5 Hz) was of great importance to investigate, but this was not possible to perform due to high noise in both indentation and force signals that appeared when applying the lower frequencies, hindering data acquisition. The results of the AFM measurements showed that the control group before and after incubation as well as the MGO group before incubation have a dependency on frequency. However, the MGO treated fibrils did not show any significant change with changing the frequency. The AFM static nanoindentation showed that no change in the indentation modulus could be detected in the current experiment due to glycation. This is inconsistent to the widespread assumption and existing data that there is a direct link between AGEs and the increased fibril stiffness. However, this result is in agreement with another study, which concluded that change in stiffness due to AGEs presence is not detected at this level and can occur at higher levels of tissue architecture.

Subsequently, dynamic tensile tests were performed on the same fibrils using the NanoTens instrument with an oscillating force at a range of frequencies lower than 1 Hz. The results suggested that the MGO treated fibrils seem to be less viscous and stiffer. Although the results showed that the MGO group has lower dissipation and larger strength than the control group, the influence of glycation could not manifest clearly on both elastic and viscoelastic properties in the current study. However, these changes between both control and test groups may be due to random sampling differences as the test group already showed differences compared to the control group before incubation in MGO solution. Another explanation can be the small sample size of both groups in both methods, which was less than 10 samples in

each group. Furthermore, due to the absence of chemical validation of cross-link formation, the glycation protocol may not have been working as intended leading to no or too few newly formed cross-links.

In conclusion, both measurement techniques proved to be very useful and provide a new perspective on the DMA (dynamic mechanical analysis) on a nanoscale. The results of both measurements correlated, and a workflow was established for both methods, which can be further improved. Clear impact of glycation could not be detected and MGO levels should be quantified in the future. Whereas the results show certain tendencies, these results need to be verified and the topic further examined. This may include the enhancement of measurement protocols and the investigation of a larger sample using a broader range of frequencies.

8 Table of Figures

9 Table of tables

Bibliography and References

1. Bailey, A.J., L. Paul Rg Fau - Knott, and L. Knott, *Mechanisms of maturation and ageing of collagen.* (0047-6374 (Print)).

2. Paul, R. and A. Bailey, *Glycation of collagen: the basis of its central role in the late complications of ageing and diabetes.* The international journal of biochemistry & cell biology, 1996. **28**(12): p. 1297-1310.

3. Gouldin, A.G., M.E. Brown, and J.L. Puetzer, *An inducible model for unraveling the effects of advanced glycation end-product accumulation in aging connective tissues.* Connective Tissue Research, 2022. **63**(4): p. 406-424.

4. Snedeker, J.G. and A. Gautieri, *The role of collagen crosslinks in ageing and diabetes - the good, the bad, and the ugly.* (2240-4554 (Print)).

5. Efremov, Y.M., T. Okajima, and A. Raman, *Measuring viscoelasticity of soft biological samples using atomic force microscopy.* Soft matter, 2020. **16**(1): p. 64-81.

6. Fratzl, P., *Collagen : structure and mechanics.* 2008: New York, NY : Springer, 2008. XVIII, 506 S., Ill., graph. Darst.

7. Varma, S., J.P. Orgel, and J.D. Schieber, *Nanomechanics of Type I Collagen.* (1542-0086 (Electronic)).

8. Svensson, R.B., et al., *Viscoelastic behavior of discrete human collagen fibrils.* (1878-0180 (Electronic)).

9. Grant, C.A., N.H. Phillips Ma Fau - Thomson, and N.H. Thomson, *Dynamic mechanical analysis of collagen fibrils at the nanoscale.* (1878-0180 (Electronic)).

10. Yamamoto, N., *Tensile strength of single collagen fibrils isolated from tendons.* European Journal of Biophysics, 2017. **5**(1): p. 1.

11. Clemmer, J., et al., *A mechanistic study for strain rate sensitivity of rabbit patellar tendon.* (1873-2380 (Electronic)).

12. Rufin, M., *Effect of clycation on surface charge and indentation stiffness of individual collagen fibrils*. 2020, Wien.

13. Kain, L., *Structural and mechanical evaluation of collagen fibrils from equine tendon: The effect of age, tendon zone and type*. 2017, Wien.

14. Sherman, V.R., W. Yang, and M.A. Meyers, *The materials science of collagen.* Journal of the mechanical behavior of biomedical materials, 2015. **52**: p. 22-50.

15. Scherübl, J., *Nanomechanical-testing of individual of collagen fibrils from an osteogenesis imperfecta mouse model*. 2018, Wien.

16. Wan, Y., et al., *Effects of ultrasound and thermal treatment on the ultrastructure of collagen fibers from bovine tendon using atomic force microscopy.* (1873-7072 (Electronic)).

17. Akhtar, R., et al., *Frequency-modulated atomic force microscopy localises viscoelastic remodelling in the ageing sheep aorta.* (1878-0180 (Electronic)).

18. Pornprasertsuk, S., et al., *Lysyl hydroxylase-2b directs collagen cross-linking pathways in MC3T3-E1 cells.* Journal of Bone and Mineral Research, 2004. **19**(8): p. 1349-1355.

19. Fessel, G., et al., *Advanced glycation end-products reduce collagen molecular sliding to affect collagen fibril damage mechanisms but not stiffness.* PloS one, 2014. **9**(11): p. e110948.

20. Amendola, P.G., R. Reuten, and J.T. Erler, *Interplay between LOX enzymes and integrins in the tumor microenvironment.* Cancers, 2019. **11**(5): p. 729.

21. Fratzl, P., *Collagen: structure and mechanics, an introduction*, in *Collagen*. 2008, Springer. p. 1-13.

22. Svensson, R.B., et al., *Effects of maturation and advanced glycation on tensile mechanics of collagen fibrils from rat tail and Achilles tendons.* Acta Biomaterialia, 2018. **70**: p. 270-280.

23. López-Guerra, E.A.-O. and S.A.-O. Solares, *On the frequency dependence of viscoelastic material characterization with intermittent-contact dynamic atomic force microscopy: avoiding mischaracterization across large frequency ranges.* (2190-4286 (Print)).

24. Shen, Z.L., et al., *Viscoelastic properties of isolated collagen fibrils.* (1542-0086 (Electronic)).

25. Haugstad, G., *Atomic force microscopy : understanding basic modes and advanced applications*. 2012: Hoboken, N.J. : Wiley, 2012. XXII, 464 S., Ill., graph. Darst., 25 cm.

26. Park Systems. *How AFM works*. 2022; Available from: https://parksystems.com/medias/nano-academy/how-afm-works.

27. Baró, A.M. and R.G. Reifenberger, *Atomic force microscopy in liquid: biological applications*. 2012: John Wiley & Sons.

28. Haugstad, G., *Atomic force microscopy: understanding basic modes and advanced applications*. 2012: John Wiley & Sons.

29. Bowen, R. and N. Hilal, *Atomic force microscopy in process engineering: An introduction to AFM for improved processes and products*. 2009: Butterworth-Heinemann.

30. AFM Workshop. *Measuring and understanding force-distance curves*. Available from: https://www.afmworkshop.com/images/datasheets/Measuring-and-understanding-force-distance-curves-v2.pdf.

31. Bansal, H.O., *Tuning of PID controllers using simulink.* International Journal of Mathematical Modeling, Simulations and Applications, 2009. **2**(3): p. 337-344.

32. Morris, V.J., A.R. Kirby, and P.A. Gunning, *Atomic force microscopy for biologists*. 2009: World Scientific.

33. Baró, A.M., *Atomic force microscopy in liquid : biological applications*. 2012: Weinheim : Wiley-VCH, 2012. XIX, 362 S., Ill., graph. Darst.

34. Nano and more GMBH. *What is Atomic Force Microscopy*. 2022; Available from: https://www.nanoandmore.com/what-is-atomic-force-microscopy?gclid=CjwKCAiA1JGRBhBSEiwAxXblwQhtbMtpeofo7iE-1KbhNcENv_ZWAqZ11kYc2Hm5qdNn8f9dSrbGaBoClNEQAvD_BwE.

35. Bruker. *QI Advanced Mode*. 2022; Available from: https://www.bruker.com/en/products-and-solutions/microscopes/bioafm/bioafm-accessories/qi-advanced-mode.html.

36. De Sousa, J., et al., *Analytical model of atomic-force-microscopy force curves in viscoelastic materials exhibiting power law relaxation.* Journal of Applied Physics, 2017. **121**(3): p. 034901.

37. Bruker. *MicroRheology Software Module*. 2020; Available from: https://www.bruker.com/en/products-and-solutions/microscopes/bioafm/bioafm-accessories/microrheology-software-module.html.

38. Tan, X., et al., *Dynamical characterization of micro cantilevers by different excitation methods in dynamic atomic force microscopy.* Review of Scientific Instruments, 2018. **89**(11): p. 115109.

39. Liu, Y., R. Ballarini, and S.J. Eppell, *Tension tests on mammalian collagen fibrils.* Interface focus, 2016. **6**(1): p. 20150080.

40. Van Der Rijt, J.A., et al., *Micromechanical testing of individual collagen fibrils.* Macromolecular bioscience, 2006. **6**(9): p. 697-702.

41. Nalbach, M., et al., *Instrument for tensile testing of individual collagen fibrils with facile sample coupling and uncoupling.* Review of Scientific Instruments, 2022. **93**(5): p. 054103.

42. Shrivastava, A., *Introduction to plastics engineering*. 2018: William Andrew.